Front. Phys. 11(1), 111204 (2016)
DOI 10.1007/s11467-015-0525-6

REVIEW ARTICLE

# Spin physics through unpolarized processes

**Zhun Lu**

*Department of Physics, Southeast University, Nanjing 211189, China*

*E-mail: zhunlu@seu.edu.cn*

*Received November 3, 2015; accepted November 22, 2015*

This article presents a review of our present understanding of the spin structure of the unpolarized hadron. Particular attention is paid to the quark sector at leading twist, namely, the quark Boer–Mulders function, which describes the transverse polarization of the quark inside an unpolarized hadron. After introducing the operator definition of the Boer–Mulders function, a detailed treatment of different non-perturbative calculations of the Boer–Mulders functions is provided. The phenomenology in Drell–Yan processes and semi-inclusive leptoproduction, including the extraction of the quark and antiquark Boer–Mulders functions from experimental data, is presented comprehensively. Finally, prospects for future theoretical studies and experimental measurements are presented in brief.

**Keywords** transverse spin, Boer–Mulders function, semi-inclusive DIS, Drell–Yan, quark model

**PACS numbers** 12.39.-x, 13.60.-r, 13.85.-t, 13.88.+3

Contents



## 1 Introduction

Understanding the spin structure of the nucleon has become one of the main tasks in QCD and hadronic physics [1–3]. Normally, the partonic structure of hadrons in high-energy scattering is described by the parton distribution functions. In the collinear picture, there are three distributions at leading-twist level: the momentum density $f_1(x)$; the longitudinal polarization, or the helicity distribution $g_1(x)$; and the transverse polarization, or the transversity distribution $h_1(x)$, with $x$ the longitudinal momentum fraction of partons. The latter two distributions are spin-dependent and are essential observables to encode the spin structure of the polarized nucleon. During the past two decades, detailed knowledge on the quark helicity distribution has been obtained from different model calculations [4–6], as well as from dedicated experimental measurements, which shed light on the parametrizations of $g_1(x)$ [7–11]. Although it is more difficult to probe the quark transversity distribution due to its chiral-odd nature, researchers have started gaining some basic information of this distribution by taking advantage of the semi-inclusive deeply inelastic scattering (SIDIS) process [12, 13].

In the last decade, it has been shown that a much more comprehensive image of the nucleon can be obtained by considering the intrinsic transverse motion of partons [14–19]. In this scenario, which is beyond the

*Special Topic: Spin Physics (Eds. Haiyan Gao & Bo-Qiang Ma).

collinear picture, besides the original three distributions, there are five more leading-twist distributions, which not only depend on $x$, but also depend on the transverse momentum $k_T$ of partons, as shown in Table 1. For this reason, they are called as the transverse momentum dependent (TMD) distribution functions. Among them, the Sivers function $f_{1T}^{\perp}(x, \boldsymbol{k}_T^2)$ [20, 21] and the Boer–Mulders function $h_1^{\perp}(x, \boldsymbol{k}_T^2)$ [15] are of particular interest. The former represents an azimuthal asymmetry of unpolarized quarks inside a transversely polarized hadron, whereas the latter, in contrast, describes a transverse-polarization asymmetry of quarks inside an unpolarized hadron. This novel structure surpasses the conventional wisdom that the partons inside an unpolarized hadron should also be unpolarized. However, for a while the very existence of the Boer–Mulders function was not as obvious. This is because, similar to its counterpart–the Sivers function, the Boer–Mulders function involves a (naively) time-reversal-odd (T-odd) correlation, which was thought to be forbidden by the time-reversal invariance of QCD [22]. For this reason, they are classified as T-odd distributions. However, later model calculations [23, 24], together with a re-examination [25] on the time-reversal argument shows that T-odd distributions actually do not vanish.

The purpose of this article is to present a review of the theoretical foundation (Section 2) and model aspects (Section 3) of the Boer–Mulders function, as well as the phenomenological approaches to access the function (Sections 4 and 5). As a TMD distribution, the Boer–Mulders function cannot be probed in inclusive leptoproduction. In addition, the chiral-odd nature of the Boer–Mulders function further complicates the experimental measurement and phenomenological analysis. That is, another chiral-odd object is required to couple with the Boer–Mulders function. Two promising processes that can be applied to access the Boer–Mulders function are the Drell–Yan (Section 4) and the SIDIS (Section 5) processes. The corresponding observables are the $\cos 2\phi$ azimuthal angular dependence of the final dilepton (in Drell–Yan) and that of the fragmented hadron (in SIDIS). The challenge in the extraction of the Boer–Mulders function is to disentangle the convolution of two chiral-odd functions from the $\cos 2\phi$ asymmetries. However, the advantage of conducting these measurements is that the hadrons in the initial or the final state do not necessarily have to be polarized. This opens a new window to study the spin structure of the nucleon through unpolarized processes!

**Table 1** The five TMD distributions appear after the intrinsic transverse momentum is introduced. The symbols U, L, and T in the first row represent the unpolarized, longitudinally and transversely polarized states of the nucleon, respectively. The symbols U, L, and T in the first column represent unpolarized, longitudinal, and transversely polarized states of quarks, respectively.

| | U | L | T |
|---|---|---|---|
| U | $f_1(x, \boldsymbol{k}_T^2)$ | | $h_1^{\perp}(x, \boldsymbol{k}_T^2)$ |
| L | | $g_1(x, \boldsymbol{k}_T^2)$ | $h_{1L}^{\perp}(x, \boldsymbol{k}_T^2)$ |
| T | $f_{1T}^{\perp}(x, \boldsymbol{k}_T^2)$ | $g_{1T}(x, \boldsymbol{k}_T^2)$ | $h_1(x, \boldsymbol{k}_T^2)$, $h_{1T}^{\perp}(x, \boldsymbol{k}_T^2)$ |

## 2 Theoretical foundation of the Boer–Mulders function

This section presents the theoretical foundation on which the Boer–Mulders function is established. The partonic structure of the nucleon may be encoded in the TMD quark-quark correlation function which has the following form [16, 17]

$$\Phi_{ij}(x, k_T) = \int \frac{\mathrm{d}\xi^- \mathrm{d}^2\boldsymbol{\xi}_T}{(2\pi)^3} \mathrm{e}^{\mathrm{i}k\cdot\xi} \langle P|\bar{\psi}_j(0)\, \mathcal{L}^{n_-}_{(0,+\infty)} \times \mathcal{L}^{n_-}_{(+\infty,\xi)}\, \psi_i(\xi)|P\rangle\Big|_{\xi^+=0}, \tag{1}$$

where $x = k^+/P^+$, with $k$ and $P$ the of momenta of the quark and nucleon, respectively. For convenience, I have adopted the light-cone coordinates $a^{\pm} = (a^0 \pm a^3)/\sqrt{2} = a \cdot n_{\mp}$ for an arbitrary four-vector $a = [a^+, a^-, \boldsymbol{a}_T]$, with the light-like vectors defined as $n_+ = [0, 1, \boldsymbol{0}_T]$ and $n_- = [1, 0, \boldsymbol{0}_T]$.

In the correlator (1) the following gauge links (Wilson lines) appear

$$\mathcal{L}^{n_-}_{(0,+\infty)} = \mathcal{L}^{n-}(0^-, \infty^-; \boldsymbol{0}_T)\mathcal{L}^{T}(\boldsymbol{0}_T, \boldsymbol{\infty}_T; \infty^-), \tag{2}$$

$$\mathcal{L}^{n_-}_{(+\infty,\xi)} = \mathcal{L}^{T}(\boldsymbol{\infty}_T, \boldsymbol{\xi}_T; \infty^-)\mathcal{L}^{n-}(\infty^-, \xi^-, \boldsymbol{\xi}_T) \tag{3}$$

to ensure the gauge-invariance of the operator definition. Here $\mathcal{L}^{n-}(a^-, b^-; \boldsymbol{c}_T)$ denotes a Wilson line running along the minus direction of the light-cone from $[a^-, 0^+, \boldsymbol{c}_T]$ to $[b^-, 0^+, \boldsymbol{c}_T]$, whereas $\mathcal{L}^{T}(\boldsymbol{a}_T, \boldsymbol{b}_T; c^-)$ is the transverse gauge-link running in the transverse direction from $[c^-, 0^+, \boldsymbol{a}_T]$ to $[c^-, 0^+, \boldsymbol{b}_T]$, in the form of path-ordered exponential:

$$\mathcal{U}^{n-}(a^-, b^-; \boldsymbol{c}_T) = \mathcal{P}\exp\left[-\mathrm{i}g\int_{a^-}^{b^-} \mathrm{d}\zeta^- A^+(\zeta^-, 0^+, \boldsymbol{c}_T)\right], \tag{4}$$

$$\mathcal{U}^{T}(\boldsymbol{a}_T, \boldsymbol{b}_T; c^-) = \mathcal{P}\exp\left[-\mathrm{i}g\int_{\boldsymbol{a}_T}^{\boldsymbol{b}_T} \mathrm{d}\boldsymbol{\zeta}_T \cdot A_T(c^-, 0^+, \boldsymbol{\zeta}_T)\right]. \tag{5}$$

The gauge-link in (4) indicates that the correlator in Eq. (1) is the one appearing in semi-inclusive DIS. The transverse gauge-link in the correlator vanishes when the transverse momentum is integrated out. However, for the

TMD correlator, the transverse gauge-link has to be included to ensure the gauge invariance of the operator definition.

For the unpolarized hadron, according to the hermiticity and parity invariance, at leading twist the correlator can be decomposed as

$$\Phi(x,k_T)=\frac{1}{2}\left\{f_1(x,k_T^2)+\mathrm{i}h_1^{\perp}(x,k_T^2)\frac{[\not{k}_T,\not{n}_+]}{2M}\right\}, \quad (6)$$

where $f_1(x,k_T^2)$ is the TMD unpolarized distribution function, and $h_1^{\perp}(x,k_T^2)$ denotes the Boer–Mulders function, which is first introduced in Ref. [15]. Using Eq. (1), the operator definition of the Boer–Mulders function becomes:

$$h_1^{\perp}(x,k_T^2)=-\frac{M}{2\varepsilon^{\alpha\rho}k_{T\rho}}\int\frac{\mathrm{d}\xi^-\mathrm{d}^2\boldsymbol{\xi}_T}{(2\pi)^3}\mathrm{e}^{\mathrm{i}k\cdot\xi}\langle P|\bar{\psi}_j(0)\times\mathcal{L}^{n-}_{(0,+\infty)}\,\mathrm{i}\sigma^{\alpha+}\gamma_5\mathcal{L}^{n-}_{(+\infty,\xi)}\,\psi_i(\xi)|P\rangle\Big|_{\xi^+=0}. \quad (7)$$

The Boer–Mulders function arises from the correlation of the quark spin $S_q$ and the quark transverse momentum:

$$\varepsilon^{\mu\nu\rho\sigma}P_\mu k_\nu S_{q\rho}n_\sigma\,. \quad (8)$$

Before the establishment of a fully gauge-invariant operator definition of quark-quark correlator given in Eq. (1), it was thought that this kind of correlation violates the time-reversal-invariant condition of QCD ($C=\mathrm{i}\gamma^2\gamma^0$ is the parity operator):

$$\Phi(x,k_T)=(-\mathrm{i}\gamma_5C)\,\Phi(x,-k_T)(-\mathrm{i}\gamma_5C). \quad (9)$$

For this reason, the Boer–Mulders function, as well as its chiral-even partner, the Sivers function [20, 21], is usually referred to as the T-odd distribution function. Therefore, for a while it was believed that T-odd distributions should vanish, constrained by time reversal invariance of QCD [22]. However, using spectator model calculation, which incorporates gluon exchange between the struck quark and the spectator remnants, Brodsky, Hwang, and Schmidt demonstrated [23, 24] that the T-odd distributions can actually be nonzero. Collins reexamined the time-reversal-invariance argument and proved that the gauge-link in the operator definition of the correlator permits nonvanishing T-odd distributions. The spectator model calculation by Brodsky *et al.* and Collins's proof are consistent, as it is found that, the summation of all final-state or initial-state interactions between the struck quark and the remnants leads to the gauge-link appearing in the operator definition of TMD distributions [26–28].

Furthermore, the presence of the gauge-link indicates that the T-odd distributions in SIDIS and Drell–Yan lepton pair production are reversed in sign:

$$h_1^{\perp}(x,k_T^2)|_{\mathrm{DY}}=-h_1^{\perp}(x,k_T^2)|_{\mathrm{DIS}}. \quad (10)$$

This is a direct consequence of the renewed condition for the time reversal invariance of the correlator:

$$\Phi^{[+]*}(x,k_T)=(-\mathrm{i}\gamma_5C)\,\Phi^{[-]}(x,-k_T)(-\mathrm{i}\gamma_5C), \quad (11)$$

where $\Phi^{[+]}$ and $\Phi^{[-]}$ are the correlators for the SIDIS process and the Drell–Yan process, respectively. Correspondingly, in Drell–Yan lepton pair production, all occurrences of $\infty^-$ in the gauge links in the operator definition (7) should be replaced by $-\infty^-$.

As a twist-2 distribution function, the Boer–Mulders function has a clear partonic probability interpretation. The distribution of quarks whose polarization is transverse (along the up direction) to the momentum of an unpolarized hadron can be expressed as [29]

$$f_{q^\uparrow/p}(x,k_T)=\frac{1}{2}\left[f_1^q(x,k_T^2)-h_1^{q\perp}(x,k_T^2)\frac{(\hat{\boldsymbol{P}}\times\boldsymbol{k}_T)\cdot\boldsymbol{S}_q}{M}\right]. \quad (12)$$

This gives the difference

$$f_{q^\uparrow/p}(x,k_T)-f_{q^\downarrow/p}(x,k_T)=-\frac{|k_T|}{M}h_1^{q\perp}(x,k_T^2)\sin(\phi_k-\phi_s) \quad (13)$$

$$=\Delta^N f_{q^\uparrow/p}(x,k_T)\sin(\phi_k-\phi_s), \quad (14)$$

such that

$$\Delta f_{q^\uparrow/p}(x,k_T)=-\frac{|k_T|}{M}h_1^{q\perp}(x,k_T^2). \quad (15)$$

Here $\Delta f_{q^\uparrow/p}(x,k_T)$ is another notation for the Boer–Mulders function advocated in Ref. [30]. Thus, the Boer–Mulders function describes the quark transverse polarization distribution in an unpolarized hadron, as depicted in Fig. 1. Since transverse polarization states are off-diagonal in the helicity basis (helicity flip), and helicity and chirality are the same at leading twist [31], the Boer–Mulders function is also classified as the chiral-odd distribution. As QCD and QED interactions conserve the helicity (in the massless limit), the measurable effect can only manifest if there is another chiral-odd object which is coupled with the Boer–Mulders function. The chiral-odd probe can be the Boer–Mulders function from another hadron. In this case the corresponding process is the unpolarized Drell–Yan process, in which a $\cos 2\phi$ asymmetry of the dilepton may be measured, with $\phi$ the azimuthal angle between the dilepton plane and the hadron plane. Another chiral-odd probe is the

**Fig. 1** Probability interpretation of the Boer–Mulders function. the vertical arrows represent the transverse polarization of the quark, the skewed arrows represent the transverse motion of the quark.

Collins function [22] that describes the TMD fragmentation of a transversely polarized quark to an unpolarized hadron. The coupling of the Boer–Mulders function and the Collins function appears in the unpolarized SIDIS process, and contributes a $\cos 2\phi_h$ angular dependence of the final-state hadron. The detailed phenomenology of unpolarized Drell–Yan and SIDIS is presented in Sections 3 and 4, respectively.

## 3 Modeling the Boer–Mulders function

Model calculation is an important approach to understanding the Boer–Mulders function. This is because the Boer–Mulders function, like other TMD distributions, corresponds to the matrix element of non-local operators sandwiched by hadron states. Therefore, it is not possible to calculate it from the first principles of QCD. Instead, the Boer–Mulders functions for the nucleon and the pion have been extensively studied in literatures [32–48] by several QCD-inspired quark models, and it has become a very active research field in spin physics. Although these models oversimplify the complexity of QCD dynamics in hadrons, studies in models provide important nonperturbative properties of the Boer–Mulders function, such as the size and sign of the Boer–Mulders function at the hadronic scale. Furthermore, model predictions also provide insight into the phenomenological parametrization of the Boer–Mulders function from experimental data. In the following sections I review the present status of model calculations of the Boer–Mulders function. The commonly used models are the spectator model [32–35, 38, 40, 46], the constituent light-cone quark model [42, 47], the bag-like model [41, 42, 48], and the large $N_c$ model [36], which are all inspired by QCD in different respects. These models have also been adopted to calculate other TMD distributions, including those that are T-even. As a T-odd TMD distribution, the Boer–Mulders function explicitly requires the presence of the gauge-link in the operator definition. This makes its calculation more complicated than that of T-even TMD distributions. Particularly, we pay more attention to the spectator model to demonstrate the essential steps on the calculation of the Boer–Mulders function.

### 3.1 Spectator model

The first model that predicts nonzero T-odd distributions is the spectator model [23]. In this model, the hadron is assumed to be composed of the active quark, which participates in the scattering process, and the spectator, which groups all the other quarks and gluons degree of freedom:

$$|H\rangle \mapsto |q\ + \text{spectator}\rangle.$$

In this way, the spectator plays the role of an on-shell quasi-particle with definite mass that truncates the sum over intermediate states, and the matrix element in the correlator can be given as [49]

$$\sum_X \int \frac{\mathrm{d}^3 \boldsymbol{P_X}}{(2\pi)^3} \delta(P_X^2 - M_X^2) \langle P|\bar{\psi}(0)|X\rangle \times \langle X|\mathcal{L}^{n_-}_{(0,+\infty)}\, \mathcal{L}^{n_-}_{(+\infty,\xi)}\, \psi(\xi)|P\rangle\,, \tag{16}$$

where $X$ represents all the possible spectators, and $P_X$ and $M_X$ are the momentum and the effective mass of the spectator. For the proton, the spectator is formed by two quarks, the so-called diquark, in the minimal Fock-state expansion. Thus, the spectator diquark can have the quantum numbers of a scalar (spin 0) isoscalar or axial-vector (spin 1) iso-vector diquark. At the tree level, the nucleon-quark-diquark scattering amplitude has the form

$$\langle P|\bar{\psi}(0)|X\rangle = \begin{cases} \bar{U}(P)\,\Upsilon_s\,\dfrac{\mathrm{i}}{\not{k}-m}\,, \\ \qquad \text{scalar diquark;} \\ \bar{U}(P)\,\Upsilon_v^\mu\,\dfrac{\mathrm{i}}{\not{k}-m}\,\varepsilon_\mu(P-k,\lambda_a)\,, \\ \qquad \text{vector diquark,} \end{cases} \tag{17}$$

where $\Upsilon_{s/v}$ denotes the nucleon-quark-diquark vertex ($s$ for the scalar diquark and $v$ for the axial-vector diquark), an effective vertex which may contain a model-dependent form factor [40],

$$\Upsilon_s(k^2) = \mathrm{i} g_s(k^2), \tag{18}$$

$$\Upsilon_v^\mu(k^2) = \mathrm{i}\frac{g_v(k^2)}{\sqrt{2}}\gamma^\mu\gamma^5, \tag{19}$$

where $\varepsilon_\mu(P-k,\lambda_a)$ is the polarization vector of the axial-vector diquark, and $g_X(k^2)$ is the form factor of the coupling. We note that a different form for $\Upsilon_v^\mu(k^2)$ was adopted in Ref. [38]:

$$\Upsilon_v^\mu(k^2) = \mathrm{i}\frac{g_v(k^2)}{\sqrt{3}}(\gamma^\mu - R_g\frac{k^\mu}{M})\gamma^5. \tag{20}$$

The literature contains several reports of variations of the spectator-diquark model applied to calculate the

Boer–Mulders function of the nucleon. The most simple case is the model that only includes the scalar diquark, which was used in the early calculations [32–34]. In Refs. [35, 38, 40], the authors employed spectator-diquark models that include both scalar and axial-vector diquarks.

Another variation is the choice of the form factor $g_X(k^2)$, as shown in the following list:

$$g_X(k^2)=\begin{cases} N_x(\text{constant } l), & \text{point-like;} \\ N_X\frac{k^2-m^2}{(k^2-\Lambda_X^2)^\alpha}, & \text{multipolar;} \\ N_X \mathrm{e}^{(k^2-m^2)/\Lambda_X^2}, & \text{exponential.} \end{cases} \tag{21}$$

The point-like coupling constant $g_X(k^2) \to N_X$ was adopted in Ref. [32], whereas the multipole form factor was applied in Refs. [35, 40] (with $\alpha = 2$ corresponding to the dipolar form factor) and Ref. [38]. The exponential or Gaussian form factor was used in Refs. [33, 34]. The parameter $\Lambda_X$ in the multipolar and exponential form factors provides a cutoff on the momentum $k$. It can eliminate the logarithmic divergences arising from $k_T$ integration when using a point-like coupling.

Finally, different choices of the polarization vector of the spin-1 axial-vector diquarks were also employed in the literature. The following list summarizes all the possibilities on the polarization sum $d^{\mu\nu} = \sum_{\lambda_a} \varepsilon^{*\mu}_{(\lambda_a)} \varepsilon^{\nu}_{(\lambda_a)}$ in different calculations [35, 38, 49, 50]:

$$d^{\mu\nu}(q)=\begin{cases} -g^{\mu\nu}+\dfrac{q^\mu q^\nu}{M_a^2} \\ -g^{\mu\nu}+\dfrac{q^\mu n_-^\nu+q^\nu n_-^\mu}{q\cdot n_-}-\dfrac{M_a^2}{[q\cdot n_-]^2}\, n_-^\mu\, n_-^\nu \\ -g^{\mu\nu} \\ -g^{\mu\nu}+\dfrac{P^\mu P^\nu}{M_a^2}. \end{cases} \tag{22}$$

In the following, I sketch the calculation of the Boer–Mulders function of the scalar diquark model with a dipolar form factor for the nucleon-quark-diquark coupling. The key ingredient in the calculation of T-odd distributions is the gauge-link appearing in the operator definition, because without it the result will be zero. Besides, it is necessary to apply a certain gauge to perform the calculation, and the final result should not depend on the gauge [26]. In the following, the Feynman gauge is employed as an example. The gauge-link can then be simplified to one running along the light-like direction $n_-$,

$$\mathcal{U}^{n_-}(0^-,\infty^-;\mathbf{0}_T) = \mathcal{P}\exp\left[-\mathrm{i}g\int_{0^-}^{\infty^-}\mathrm{d}\zeta^- A^+(\zeta^-,0^+,\mathbf{0}_T)\right]. \tag{23}$$

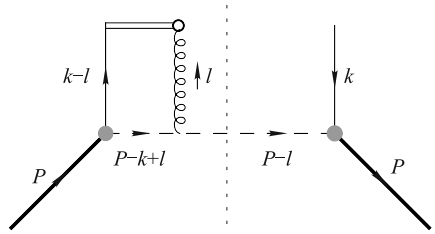


**Fig. 2** The Feynman diagram used to calculate the Boer–Mulders function in the spectator-diquark model.

Expanding the above exponential to its first nontrivial order gives the eikonal propagator:

$$\frac{1}{-l^-+\mathrm{i}\varepsilon}. \tag{24}$$

This corresponds to the so-called one-gluon exchange approximation. The diagram used to calculate the Boer–Mulders function in the spectator-diquark model is shown in Fig. 2. The double line represents the eikonal line from the gauge link, whereas the open circle denotes the eikonal vertex. The Feynman rule for the latter is given as $-\mathrm{i}e_c\, n_-^\rho$, with $e_c$ the color charge of the quark. With the above ingredients, the correlator for the scalar diquark component has the form:

$$\Phi_s^{(1)}(x,\boldsymbol{k}_T) \equiv -\mathrm{i}e_c N_s^2 \frac{(1-x)^2}{64\pi^3(P^+)^2}\frac{-\mathrm{i}\Gamma_s^+}{(k^2-\Lambda_s^2)^2} \times\int\frac{\mathrm{d}^2\boldsymbol{l}_T}{(2\pi)^2}\frac{[(\not{k}-\not{n}+m)(\not{P}+M)(\not{k}+m)]}{\boldsymbol{q}_T^2\left[(\boldsymbol{k}_T-\boldsymbol{l}_T)^2+L_s^2\right]^2}, \tag{25}$$

with $l^+ = 0$, and $\Gamma_s^\mu$ being the vertex between the gluon and the scalar diquark:

$$\Gamma_s^\mu = \mathrm{i}e_c(2P-2k+l)^\mu. \tag{26}$$

Using Eqs. (7) and (25) enables the final result from the scalar-diquark contribution to the Boer–Mulders function to be obtained:

$$h_1^{\perp\,(s)}(x,\boldsymbol{k}_T^2) = -\frac{g_s^2}{4}\frac{M\,e_c^2}{(2\pi)^4}\frac{(1-x)^3\,(m+xM)}{L_s^2\,(\boldsymbol{k}_T^2+L_s^2)^3} \tag{27}$$

with $L_s^2 = k^2-\Lambda_s^2 = xM_s^2+(1-x)m^2-x(1-x)M^2$. It is of interest to point out that for scalar diquarks the spectator model gives the same result for the Sivers and the Boer–Mulders functions, independent of the choice of the nucleon-quark-diquark form factor.

Obtaining the flavor dependence on the Boer–Mulders function requires inclusion of the contribution from the axial-vector diquark. The calculation is similar to the case of the scalar diquark. For details the readers can refer to Refs. [38, 40]. In Figs. 3 and 4, I show the first $k_T$-moment of the Boer–Mulders functions

$$h_1^{\perp(1)} = \int \mathrm{d}^2\boldsymbol{k}_T\frac{\boldsymbol{k}_T^2}{2M^2}h_1^\perp(x,\boldsymbol{k}_T^2) \tag{28}$$

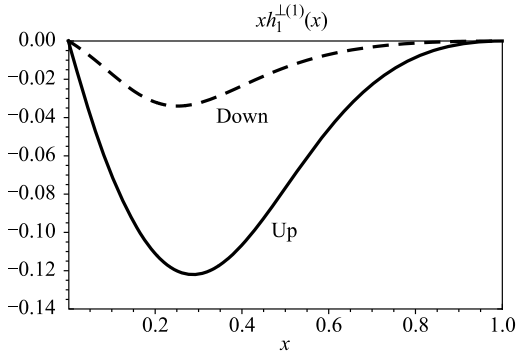


**Fig. 3** The first $k_T$-moment of the Boer–Mulders function for the $u$ and $d$ quarks inside the proton, calculated in Ref. [40] in a spectator model including the axial-diquark model. Reproduced from Ref. [40].

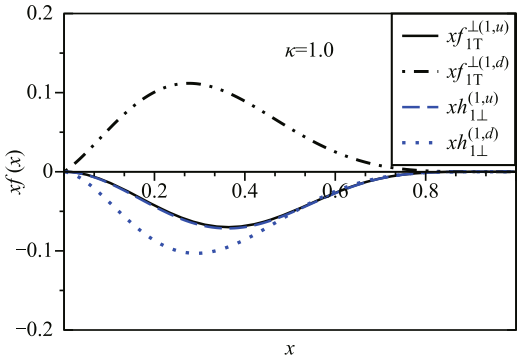


**Fig. 4** The Boer–Mulders function for the $u$ (*dashed line*) and $d$ (*dotted line*) quarks inside the proton, calculated in Ref. [38]. The results are compared with another T-odd distribution, the Sivers function. Reproduced from Ref. [38].

for the $u$ and $d$ quarks inside the proton calculated in two different spectator models, i.e., that in Ref. [40] and that in Ref. [38], respectively.

An equivalent way to perform the calculation in a spectator model is to apply the light-front formalism, in which the TMDs may be interpreted in terms of overlap of light-cone wave functions (LCWFs) for the diquark [40, 43, 50, 51]. For the Boer–Mulders function, the expression in the overlap representation has the form [40, 52]

$$\frac{(\hat{\boldsymbol{S}}_{qT}\times\boldsymbol{k}_T)\cdot\hat{\boldsymbol{P}}}{M}\,h_1^{\perp}(x,\boldsymbol{k}_T^2)=\int\frac{\mathrm{d}^2\boldsymbol{k}'_T}{16\pi^3}\times\sum_{\lambda_N,\,\lambda_X}\psi^{\lambda_N\,*}_{\uparrow\lambda_X}(x,\boldsymbol{k}_T)\,G(x,\boldsymbol{k}_T,\boldsymbol{k}'_T)\,\psi^{\lambda_N}_{\downarrow\lambda_X}(x,\boldsymbol{k}'_T)+\text{h.c.},\tag{29}$$

where $G(x,\boldsymbol{k}_T,\boldsymbol{k}'_T)$ is the FSI kernel, and $\psi^{\lambda_N}_{\lambda_q\lambda_X}$ denotes the LCWF for the quark-diquark system. Apparently, the Boer–Mulders function requires the quark helicity to be flipped from the initial to the final state, whereas the nucleon helicity remains unchanged. This indicates that the LCWFs in the initial and the final states differ by $\Delta L_z=1$, with $L_z$ the orbital angular momentum of the quark. Therefore, studying T-odd distributions like the Boer–Mulders function might also obtain information of the quark orbital motion.

### 3.2 Constituent quark model

In Ref. [47], an alternative approach, the light-cone constituent quark (LCCQ) model, was applied to calculate the Boer–Mulders function. The LCCQ model is also motivated by the light-front formalism. In the infinite momentum frame, or equivalently the light-front frame, which is suitable to study a fast moving nucleon, it is natural to describe the nucleon using the light-cone Fock state expansion of its wave function. Thus, the hadronic state can be decomposed in terms of $n$-parton Fock states with coefficients representing the momentum LCWF of the $n$ partons [53]:

$$|H,\Lambda\rangle=\sum_{n=1}^{\infty}\sum_{\lambda_i\in n}\int\left[\mathrm{d}x_i\mathrm{d}^2k_{\perp i}\right]\,\Psi^{\Lambda}_{n/H}(x_i,k_{\perp i},\lambda_i)\times|n:x_i,k_{\perp i},\lambda_i\rangle.\tag{30}$$

In principle, such an expansion contains an infinite number of LCWFs. In phenomenological calculations, a more practical way is to consider the Fock states that contain the three constituent quarks ($n=3$). For the proton, it is possible to write the $uud$ component of the light-cone state as

$$|P,\Lambda\rangle_{uud}=\sum_{\lambda_i,c_i}\int d[1]d[2]d[3]\,\Psi^{\Lambda,[f]}_{uud}(\{x_i,\boldsymbol{k}_{i\perp};\lambda_i\})\times\frac{\epsilon^{ijk}}{\sqrt{6}}b^{\dagger\,u}_{i,\,\lambda_1}(1)b^{\dagger\,u}_{j,\,\lambda_2}(2)b^{\dagger\,d}_{k,\,\lambda_3}(3)|0\rangle\,.\tag{31}$$

The LCWF $\Psi^{\Lambda,[f]}_{uud}(\{x_i,\boldsymbol{k}_{i\perp};\lambda_i\})$ in the above equation can be decomposed into momentum-dependent and spin-dependent parts using the $SU(3)$ spin-flavor symmetry of the nucleon wave function

$$\Psi^{\Lambda,[f]}_{uud}(\{x_i,\boldsymbol{k}_{i\perp};\lambda_i\})=\tilde{\psi}(\{x_i,\boldsymbol{k}_{i\perp}\})\frac{1}{\sqrt{3}}\tilde{\Phi}_{\Lambda}(\lambda_1,\lambda_2,\lambda_3).\tag{32}$$

The spin-dependent part $\tilde{\Phi}_{\Lambda}(\lambda_1,\lambda_2,\lambda_3)$ is obtained by a Melosh–Wigner rotation, which transforms the instant form of the spin eigenstates for quarks to the light-front helicity eigenstates. For a proton with spin $J_z=+1/2$, the Melosh-Wigner rotation generates the wave function amplitudes that have different orbital angular momentum: $|P\uparrow\rangle^{l_z}_{uud}$, with $l_z=0,\pm1,2$. Therefore, the P-wave and D-wave are present in the decomposition, even if the original (instant-form) wave function only contained S-wave components.

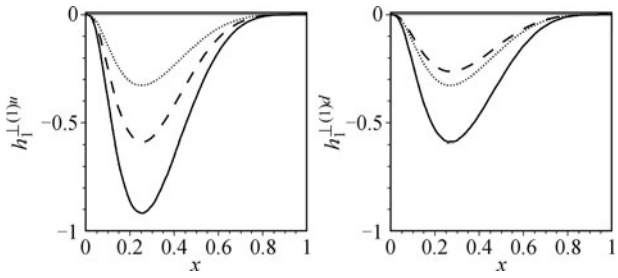


**Fig. 5** The first $k_T$-moment of the Boer–Mulders function for the $u$ (left panel) and $d$ (right panel) quarks, calculated by the LCCQM in Ref. [47]. The dashed curves show the contribution from the interference of $S$ and $P$ waves, and the dotted curves correspond to the contribution from the interference of $P$ and $D$ waves. The solid curves are the total results, the sum of all the partial-wave contributions. Reproduced from Ref. [47].

In Ref. [47], the Boer–Mulders function was calculated by inserting the LCWF decomposition of the proton (31) into Eq. (7). The gauge link was expanded to one loop to produce the final-state interaction between the active quark and the spectator quark. In this calculation the authors applied the light-cone gauge $A^+ = 0$ tailored to the light-cone quark model. Figure 5 shows the first $k_T$-moment of the Boer–Mulders function in the LCCQM, which contains the contributions from the interference of $S$ and $P$ waves and the interference of $P$ and $D$ waves. Particularly, the latter predominantly provides the contribution (60% of the total result) to $h_1^{\perp(1)}$ of the down quark.

### 3.3 Bag model

Another class of the quark model used to calculate the Boer–Mulders function is the bag model. In the simplest version of the bag model, the nucleon is described as three non-interacting massless quarks that satisfy a certain boundary condition. On the one hand, the bag model incorporates an SU(6) spin-flavor structure; on the other hand, it is the only quark model that manifests the confinement nature of the nucleon. An important feature of the bag model is that it can introduce the nucleon wave function that contains both S wave and D wave components. This is crucial in the calculation of the T-odd distribution functions, since the interference between them can generate the phase needed for the nonvanishing result after the FSI is included. The first bag-model calculation on the Boer–Mulders function was performed in Ref. [41], and a new calculation was given in Ref. [42]. As in the original bag model there is no explicit gluon degree of freedom, in these calculations, the effect of the gauge link is simulated by introducing a one-gluon exchange. In Ref. [41], the result shows that the size of the Boer–Mulders function of the up quark is twice as large as that of the down quark. and the signs for both quark flavors are negative. In Ref. [42] the authors considered the quark helicity flipped term that was not taken into account in Ref. [41]. The additional term reduces the size difference between the Boer–Mulders function of the up and down quarks.

### 3.4 Discussion on different model results

As shown in the previous subsection, although different models predict different quantitative results for the Boer–Mulders function, the results show that the size of the Boer–Mulders function is significant in the valence region. Particularly, all the models demonstrate that the signs of $h_1^\perp$ in DIS for the $u$ and $d$ flavors are both negative. In an early spectator model calculation with axial-vector diquarks, it was originally found that $h_1^\perp$ has a different sign for the $u$ and $d$ quarks [35]. The result was later corrected by the authors of Ref. [38], in which a spectator model established in previous papers [46] was applied, showing that the sign of the Boer–Mulders function for both quark flavors should be the same. This finding was confirmed in an updated calculation on $h_1^\perp$ in Ref. [40], The calculation in the constituent model [42, 47] and the bag model [41, 42] yield the same result on the sign of $h_1^\perp$.

The same sign feature of the Boer–Mulders function may be explained from a model-independent analysis according to the expansion in powers of $1/N_C$ in QCD, with $N_c$ being the number of colors. The expansion in leading order predicts that $h_1^{\perp u} = h_1^{\perp d}$. This is also in qualitative agreement with the pattern predicted by the quark helicity-flip GPD $\bar{E}_T$ in lattice simulations [54] and in different models [39, 55], which shows that all the Boer–Mulders functions are alike.

The model calculation of the Boer–Mulders function has been extended to the case of pion. The first model applied to calculate the Boer–Mulders function for the pion (denoted by $h_{1\pi}^\perp$) is the spectator model [43, 45, 46], in which the antiquark plays the role of the spectator particle. In Refs. [43] and [45], the gauge-link was taken into account by the one-gluon exchange approximation, while in Ref. [46], and the authors included higher-order gluonic contributions from the gauge link by applying nonperturbative eikonal methods. Recently, $h_{1\pi}^\perp$ was also calculated by the light-cone constituent quark model [56] and the bag model [48]. Due to the isospin asymmetry, $h_{1\pi}^\perp$ for the two valence quarks inside the pion are the same in size and sign.

It is worth pointing out that an intuitive relation between the Boer–Mulders function and the combination of chiral-odd generalized parton distributions in impact

parameter space was proposed in Refs. [57, 58]:

$$h_1^{\perp q} \leftrightarrow -\left(\mathcal{E}_T^q + 2\tilde{\mathcal{H}}_T^q\right)', \tag{33}$$

This connection between two types of parton distributions is the analogue of a corresponding relation involving the Sivers function [59, 60]. In the field-theoretical approach such a relation can be made quantitative in the framework of spectator models [52, 61, 62] However, as far as current knowledge goes, a general model-independent relation does not exist [45, 63].

## 4 The $\cos 2\phi$ angular dependence in the unpolarized Drell–Yan process

The Drell–Yan process [64–66]

$$h_1(P_1) + h_2(P_2) \to l^+(\ell) + l^-(\ell') + X \tag{34}$$

has been recognized as an important tool to probe the internal structure of hadrons. An intriguing observable in Drell–Yan is the angular distribution of the final-state dilepton when the transverse momentum of the dilepton $Q_T$ is measured. The general form of the angular differential cross section for unpolarized Drell–Yan process can be written as

$$\frac{1}{\sigma}\frac{\mathrm{d}\sigma}{\mathrm{d}\Omega} = \frac{3}{4\pi}\frac{1}{\lambda+3}\Big(1 + \lambda\cos^2\theta + \mu\sin^2\theta\cos\phi + \frac{\nu}{2}\sin^2\theta\cos 2\phi\Big). \tag{35}$$

Here $\phi$ is the azimuthal angle of the hadron plane with respect to the lepton plane in the center of mass (c.m.) frame of the dilepton. A commonly used c.m. frame is the Collins–Soper frame [67], in which the $z$-axis is along the bisector of the momenta $P_1$ and $-P_2$, as shown in Fig. 6. Some other reference frames have also been adopted in the literature, such as the Gottfried–Jackson frame [68] ($z$-axis is along beam momentum) and the $u$-channel frame ($z$-axis is along target momentum). In this article, the Collins–Soper frame will be used.

In Eq. (35), $\lambda$, $\mu$, and $\nu$ are the coefficients describing the sizes of different angular dependence. Of particular interest, $\nu$ denotes the asymmetry of the $\cos 2\phi$ azimuthal angular distribution of the dilepton. Early theoretical study on the angular distribution of the Drell–Yan process was carried out by Lam and Tung [69]. They proved a relation for $\lambda$ and $\nu$ up to the leading order of QCD: $1 - \lambda - 2\nu = 0$, the so-called Lam–Tung relation, which is an analogy of the Callan–Gross relation in DIS.

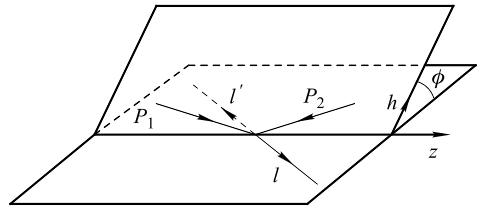


**Fig. 6** Kinematical configuration in the Collins–Soper frame [67].

The angular dependence was then measured in the process $\pi^- N \to \mu^+\mu^- X$ by the NA10 Collaboration [70, 71] and the E165 Collaboration [72], with $N$ denoting a nucleon in the deuterium or tungsten target, and for a $\pi^-$ beam with energies of 140, 194, 286 GeV [70, 71], and 252 GeV [72]. The experimental data showed a large value of $\nu$, near 30% in the region $Q_T \sim 3$ GeV. This demonstrates a clear violation of the Lam–Tung relation. The measurement on the process $\pi^- N \to \mu^+\mu^- X$ has triggered a number of theoretical and experimental studies. It is known that gluon radiation processes may give rise to a non-zero $\cos 2\phi$ asymmetry, which in the case of $q\bar{q}$ annihilation dominance is given by $\nu = Q_T^2/(M^2 + 3Q_T^2/2)$ [73]. However, the analysis in Refs. [70, 71, 74] showed that the magnitude and the $Q_T$ dependence of the asymmetry cannot be explained up to next-to-leading order perturbative QCD correction from gluon radiations. Furthermore, $\nu$ does not receive large corrections from resummation at small $Q_T$ [75]. Other proposals have been suggested to explain the observed $\cos 2\phi$ asymmetry in the unpolarized Drell–Yan process. In Ref. [76], an approach using coherent states is proposed. This can describe the $\cos 2\phi$ data, but it cannot describe the function $\mu$ in a satisfactory manner. Alternatively, the higher twist effect to the $\cos 2\phi$ asymmetry is studied in Refs. [77–79], following the $1/Q^2$ term discussed by Berger and Brodsky [80–82]. There, the higher twist effect is modeled using a pion distribution amplitude in Ref. [77]. However, it seems to fall short in explaining the large values as found for $\nu$. In Ref. [74] factorization breaking correlations between the incoming quark and antiquark are assumed in order to account for the large $\cos 2\phi$ dependence.

If the intrinsic transverse momentum of the initial quarks is taken into account, the $\cos 2\phi$ dependence may be naturally explained by the coupling of two Boer–Mulders functions from each hadron. This is the idea proposed by Boer [83]. Inserting the correlator (6) into the hadronic tensor in the Drell–Yan process, one can obtain the tree-level result of the unpolarized Drell–Yan cross section at leading-twist

$$\frac{\mathrm{d}\sigma(H_1H_2\to l^+l^-X)}{\mathrm{d}\Omega\mathrm{d}x_1\mathrm{d}x_2\mathrm{d}^2\boldsymbol{q}_T} = \frac{\alpha^2}{3Q^2}\sum_{q,\bar{q}}\left\{A(y)\mathcal{F}[f_1^q f_1^{\bar{q}}] + B(y)\cos 2\phi\mathcal{F}\left[((2\hat{\boldsymbol{h}}\cdot\boldsymbol{k}_{1T}\hat{\boldsymbol{h}}\cdot\boldsymbol{k}_{2T}) - (\boldsymbol{k}_{1T}\cdot\boldsymbol{k}_{2T}))\frac{h_1^{\perp q}h_1^{\perp\bar{q}}}{M_1M_2}\right]\right\}. \tag{36}$$

Here, the notation

$$\mathcal{F}[f\bar{f}] = \int \mathrm{d}^2\boldsymbol{k}_{1T}\mathrm{d}^2\boldsymbol{k}_{2T}\delta^2(\boldsymbol{k}_{1T}+\boldsymbol{k}_{2T}-\boldsymbol{q}_T)f(x_1,\boldsymbol{k}_{1T}^2)\bar{f}(x_2,\boldsymbol{k}_{2T}^2) \tag{37}$$

is used. The first term in Eq. (36) is azimuthal independent, whereas the second term clearly has a $\cos 2\phi$ azimuthal dependent term, which contributes to the asymmetry $\nu$. In the context of QCD, each term in Eq. (36) can be extended to a factorized form in the framework of TMD factorization [84]. The difference between the perturbative QCD correction and the Boer–Mulders effect is that the former is suppressed by the inverse hard scale $Q$, whereas for the latter the relevant scale is the nonperturbative hadronic scale, such as the hadron mass. It is also necessary to point out that the $\cos 2\phi$ asymmetries may be explained by the twist-three quark-gluon correlations in collinear factorization [85], which is consistent with the Boer–Mulders effect in the TMD factorization approach in the intermediate energy scale $\Lambda_{\rm QCD} \ll Q_T \ll Q$.

A considerable volume of phenomenological work has been proposed to understand the $\cos 2\phi$ asymmetry in an unpolarized Drell–Yan process based on the Boer–Mulders effect [32, 37, 44, 56, 86–103]. Particularly, Boer [83] argued that it can account for the observed $\cos 2\phi$ asymmetries observed in unpolarized $\pi N$ Drell–Yan processes [70–72]. This was quantitatively confirmed in Ref. [87], where $h_1^\perp$ of the nucleon and the pion were calculated in spectator models, showing that the $Q_T$ dependence of the $\cos 2\phi$ asymmetry can be reproduced fairly well. Besides, the measurements [104, 105] on the $\cos 2\phi$ asymmetry in the unpolarized $pp$ and $pd$ Drell–Yan processes have been performed by the E866/Nusea Collaboration in recent years. The data from nucleon-nucleon collision provide great opportunity to extract the Boer–Mulders function in the proton. Three different parameterizations [96, 99, 100] were adopted to fit those data to obtain the quark and antiquark Boer–Mulders function, based on the expressions for the $\cos 2\phi$ asymmetries $\nu$ in $pp$ and $pD$ Drell–Yan processes:

$$\nu_{pp} = \frac{2\mathcal{F}[\chi\,(e_u^2\,h_1^{\perp,u}\,h_1^{\perp,\bar{u}} + e_d^2\,h_1^{\perp,d}\,h_1^{\perp,\bar{d}})] + (q\leftrightarrow\bar{q})}{\mathcal{F}[e_u^2\,f_1^u f_1^{\bar{u}} + e_d^2 f_1^d f_1^{\bar{d}}] + (q\leftrightarrow\bar{q})}, \tag{38}$$

$$\nu_{pD} = \frac{2\mathcal{F}[\chi\,(e_u^2 h_1^{\perp,u} + e_d^2 h_1^{\perp,d})(h_1^{\perp,\bar{u}} + h_1^{\perp,\bar{d}})] + (q\leftrightarrow\bar{q})}{\mathcal{F}[(e_u^2 f_1^u + e_d^2 f_1^d)(f_1^{\bar{u}} + f_1^{\bar{d}})] + (q\leftrightarrow\bar{q})}, \tag{39}$$

with $\chi$ defined as

$$\chi = ((2\hat{\boldsymbol{h}}\cdot\boldsymbol{k}_{1T}\hat{\boldsymbol{h}}\cdot\boldsymbol{k}_{2T}) - (\boldsymbol{k}_{1T}\cdot\boldsymbol{k}_{2T})). \tag{40}$$

These parameterizations and the corresponding results are reviewed below.

### 4.1 Parametrization in Ref. [96]

The first extraction was given in Ref. [96], in which the TMD distribution $h_1^\perp(x,\boldsymbol{k}_T^2)$ is factorized to $x$ and $k_T$ dependent parts

$$h_1^{\perp,q}(x,\boldsymbol{k}_T^2) = h_1^{\perp,q}(x)\frac{\exp(-\boldsymbol{k}_T^2/k_{bm}^2)}{\pi k_{bm}^2}. \tag{41}$$

Here, the parametrization contains a Gaussian model for the transverse momentum dependence of the Boer–Mulders functions, with width $k_{bm}^2$. The $x$-dependence of the Boer–Mulders functions is modeled to relate its behavior with that of the unpolarized distribution functions:

$$h_1^{\perp,q}(x) = H_q\,x^c\,(1-x)\,f_1^q(x), \tag{42}$$

where $f_1^q(x)$ is the unpolarized integrated distribution function. Therefore in this fit, there are six parameters $H_u$, $H_d$, $H_{\bar{u}}$, $H_{\bar{d}}$, $p_{bm}^2$, and $c$. The factor $(1-x)$ is included to ensure the correct large-$x$ behavior [106] for $h_1^\perp$ compared with the unpolarized distribution. The small–$x$ behavior of $h_1^\perp$ with respect to $f_1(x)$ is modeled by $x^c$. The TMD unpolarized distribution function $f_1(x,\boldsymbol{k}_T^2)$ is also given in the Gaussian form

$$f_1^q(x,\boldsymbol{k}_T^2) = f_1^q(x)\,\frac{\exp(-\boldsymbol{k}_T^2/k_{unp}^2)}{\pi\,p_{unp}^2}. \tag{43}$$

where $k_{unp}^2$ is the mean squared transverse momentum of the unpolarized quarks, and is assumed to be flavor independent. In Ref. [96], $k_{unp}^2$ is chosen as $k_{unp}^2 = 0.25\ \mathrm{GeV}^2$, a value which was obtained by fitting the $\cos\phi$ azimuthal dependence of the SIDIS unpolarized cross section [107].

Using the expression (39), the parametrization form in Eq. (42) was used to fit [96] the E866/NuSea $pd$ Drell–Yan data. The best fitted values for the parameters are shown in Table 2. Note that the results for the parameters $H_q$ given in Table 2 are obtained for the Drell–Yan process. The corresponding Boer–Mulders functions are obtained in SIDIS by reversing their signs [25]. Therefore, the values of $H_u$ and $H_d$ agree with the expectation that the Boer–Mulders functions for up and down quarks in SIDIS are negative and have the same sign. It is also necessary to emphasize that the Boer–Mulders functions extracted in Ref. [96] are within the positivity bound [108]

**Table 2** Best fitted values of the Boer–Mulders functions in Ref. [96].

| | |
|---|---|
| $H_u$ | 3.99 |
| $H_d$ | 3.83 |
| $H_{\bar{u}}$ | 0.91 |
| $H_{\bar{d}}$ | –0.96 |
| $p^2_{bm}$ | 0.161 |
| c | 0.45 |
| $\chi^2/d.o.f.$ | 0.79 |

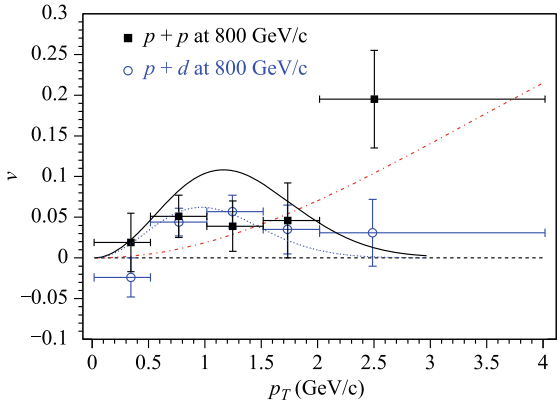


**Fig. 7** The $\cos 2\phi$ distribution $\nu$ calculated with parametrization of the Boer–Mulders functions deduced from the fit to the $p+d$ Drell–Yan data [104] in Ref. [96]. The dotted curve and the solid curves represent the result in the $pd$ and $pp$ Drell–Yan processes in the kinematic region of E866/NuSea, respectively. The calculations are compared with the E866/NuSea $pd$ [104] and $pp$ data [105]. The dot-dashed curve is the contribution from perturbative QCD.

$$\frac{|p_T h_1^{\perp}(x,\boldsymbol{k}_T^2)|}{M} \leqslant f_1(x,\boldsymbol{k}_T^2). \tag{44}$$

Figure 7 shows the $\cos 2\phi$ angular dependence $\nu$ vs. $Q_T$ in the $pd$ Drell–Yan process (dotted curve) calculated from Boer–Mulders functions parameterized in Ref. [96]. The prediction on $\nu$ in the $pp$ Drell–Yan process is also presented by the solid curve, and is compared with the E866/NuSea measurement (open circles) [105].

### 4.2 Parametrization in Ref. [99]

After the release of the $pp$ Drell–Yan data by the E866/NuSea Collaboration, an updated extraction of the Boer–Mulders functions was presented in Ref. [99], which was developed from the parametrization in Ref. [96]. In this extraction, a new parametrization form was proposed on the $x$-dependence of the Boer–Mulders functions:

$$h_1^{\perp q}(x) = H_q\, x^{c_q}\,(1-x)^b\, f_1^q(x), \tag{45}$$

Here, the large-$x$ dependence of the Boer–Mulders functions is modeled by $(1-x)^b$, with $b$ being flavor dependent, which differs from the previous fit [96] in which the large-$x$ dependence is $1-x$. Moreover, the small-$x$ behavior $x^{c_q}$ is relaxed to be flavor dependent.

As deduced from Eqs. (38) and (39), $H_u$, $H_d$, $H_{\bar{u}}$, and $H_{\bar{u}}$ always appear as combinations of two of them; hence, three independent coefficients can be defined

$$H_1 = H_u\, H_{\bar{u}}, \quad H_2 = H_d\, H_{\bar{d}}, \quad H_3 = H_u\, H_{\bar{d}}, \tag{46}$$

where the last combination $H_{\bar{u}}\, H_d$ is determined by $H_{\bar{u}}\, H_d = H_1 H_2/H_3$. In Ref. [99], the coefficients $H_1$, $H_2$, and $H_3$ were adopted as the parameters in the fit, instead of $H_q$. Therefore, there are nine free parameters that were applied to fit the E866/NuSea $p+p$ and $p+d$ data of the low $Q_T$ region ($Q_T < 2.0$ GeV). The best fit results and the errors for the parameters are as follows:

$$H_1 = 0.62^{+0.52}_{-0.29}, \quad H_2 = 1.45^{+1.30}_{-1.12}, \quad H_3 = 0.61^{+0.50}_{-0.55},$$
$$c_u = 0.63^{+0.53}_{-0.21}, \quad c_d = 0.47^{+0.36}_{-0.39}, \quad c_{\bar{u}} = 0.07^{+0.06}_{-0.05},$$
$$c_{\bar{d}} = 0.75^{+0.72}_{-0.52}, \quad b = 0.17^{+0.15}_{-0.14}, \quad p^2_{bm} = 0.173^{+0.027}_{-0.033}.$$

The $\chi^2$ of this fit is 35.95 for 52 data points, resulting in $\chi^2/d.o.f = 0.84$.

The possible range of coefficients $H_q$ is obtained from the values of $H_1$, $H_2$ and $H_3$, by employing the positivity bound [108] for $h_1^{\perp q}(x,\boldsymbol{k}_T^2)$ for the entire $x$ and $\boldsymbol{k}_T$ regions:

$$\frac{|k_T h_1^{\perp q}(x,\boldsymbol{k}_T^2)|}{M} \leqslant f_1^q(x,\boldsymbol{k}_T^2), \tag{47}$$

then the ranges for $H_q$ are

$$H_u = 0.59^{+0.64}_{-0.31}, \quad H_d = 1.37^{+1.53}_{-0.72},$$
$$H_{\bar{u}} = 1.10^{+1.21}_{-0.57}, \quad H_{\bar{d}} = 1.08^{+1.18}_{-0.56}. \tag{48}$$

The central value for $H_q$ shown above is obtained from the geometric mean values of the upper and lower limits for $H_q$: $H_q^{\rm cen} = \sqrt{H_q^{\rm max} H_q^{\rm min}}$. In a previous fit [96], the variation range of $H_q$ allowed by the positivity bound was described by the coefficient $\omega$, namely, that the substitution $H_q \to \omega H_q$ for $q = u$, $d$, and $H_q \to \frac{1}{\omega} H_q$ for $q = \bar{u}$, $\bar{d}$ will not change the result. In the new fit, the range of $\omega$ is $0.48 < \omega < 2.1$, and central values for $H_q$ correspond to $\omega = 1$. The first $\boldsymbol{k}_T^2$-moments of the Boer–Mulders functions in the fit are shown in Fig. 8.

### 4.3 Parametrization in Ref. [100]

In Ref. [100], the $pd$ and $pp$ data were applied to extract the antiquark Boer–Mulders functions $h_1^{\perp\bar{u}}$ and $h_1^{\perp\bar{d}}$. In that work, the authors assumed that $h_1^{\perp\bar{q}}$ is proportional to the Sivers function $f_{1T}^{\perp}$, following the parametrization [109] on the quark Boer–Mulders function from SIDIS

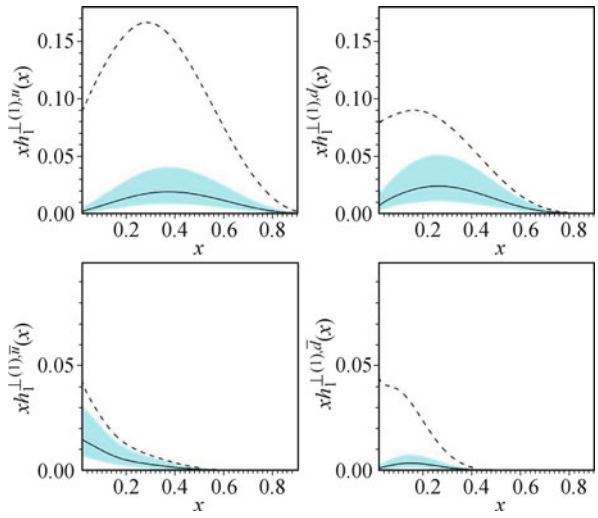

**Fig. 8** The first $\boldsymbol{k}_T$-moment of Boer–Mulders functions for $u$, $d$, $\bar{u}$ and $\bar{d}$ quarks for $Q^2 = 1$ GeV$^2$ from the parametrization in Ref. [99]. The solid lines show the central value of the distributions, the shadows depict the variation ranges of $x\,h_1^{\perp\,(1)\,q}(x)$ allowed by the positivity bound. The dashed lines show $\frac{\langle p_T\rangle_{un}}{2M} x\,f_1^{\,q}(x)$.

data. Explicitly, the antiquark Boer–Mulders functions are parameterized as

$$h_1^{\perp\bar{q}}(x,k_T^2) = N_{\bar{q}}\,x^{\alpha_{\bar{q}}}(1-x)^{\beta_{\bar{q}}}\,\mathrm{e}^{-k_T^2/\mu^2}\,\bar{f}_1^q(x,k_T^2)\,. \quad (49)$$

Here, the values of the parameters $\alpha, \beta$, and $\mu$ are taken from the antiquark Sivers distributions, and the normalization coefficients $N_{\bar{u}}$ and $N_{\bar{d}}$ are fitted to the data.

As opposed to the fit in Refs. [96, 99], in the analysis presented in Ref. [100] the quark Boer–Mulders functions were not fitted directly from Drell–Yan data. Instead, they were adopted from a previous fit to the $\cos 2\phi$ asymmetry in SIDIS [109], which is reviewed in the next section.

The last ingredient in the analysis of Ref. [100] is the quark and antiquark transverse momenta in the two hadrons, $\langle k_{1T}^2\rangle$ and $\langle k_{2T}^2\rangle$, which are taken to be equal to each other, $\langle k_T^2\rangle \equiv \langle k_{1T}^2\rangle = \langle k_{2T}^2\rangle$. In Ref. [100], the authors choose two different values for them:

$$\begin{aligned}&\text{Fit 1: } \langle k_T^2\rangle = 0.25\ \text{GeV}^2\,;\\ &\text{Fit 2: } \langle k_T^2\rangle = 0.64\ \text{GeV}^2\,,\end{aligned} \quad (50)$$

corresponding to two different fits. The smaller value, 0.25 GeV$^2$, was used in the analysis of the Boer–Mulders effect on the $\cos 2\phi$ asymmetry in SIDIS [109], and is taken from the study of the Cahn effect of Ref. [107]. The larger value, 0.64 GeV$^2$, was obtained in the analysis [110] of $pp$ scattering data at $\sqrt{s} \simeq 20$ GeV. The larger value is close to the results of a phenomenological study of the transverse-momentum dependence of DY cross sections [111].

The values of the parameters of the antiquark distributions in the two fits are presented in Table 3. The first

**Table 3** Parameters of the Boer–Mulders antiquark distributions in Ref. [100].

| $\alpha_{\bar{u}} = \alpha_{\bar{d}} = 0.79$, $\beta_{\bar{u}} = \beta_{\bar{d}} = 3.46$, $\mu^2 = 0.34$ GeV$^2$ | | | |
|---|---|---|---|
| Fit 1 | $N_{\bar{u}} = 3.6 \pm 1.0$ | $N_{\bar{d}} = 1.7 \pm 1.4$ | $\langle k_T^2\rangle = 0.25$ GeV$^2$ |
| Fit 2 | $N_{\bar{u}} = 6.4 \pm 1.7$ | $N_{\bar{d}} = 3.0 \pm 2.4$ | $\langle k_T^2\rangle = 0.64$ GeV$^2$ |

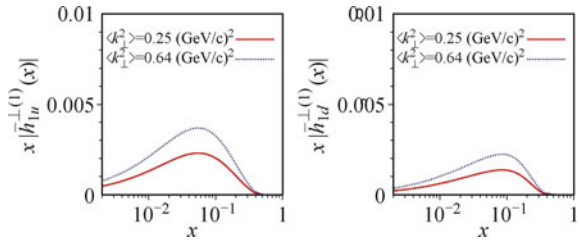

**Fig. 9** The first $k_T$-moments of the antiquark distributions from Fit 1 (*solid curves*) and Fit 2 (*dashed curves*) in Ref. [100].

$k_T^2$ moments of the antiquark distributions from Fit 1 (solid curves) and Fit 2 (dashed curves) are shown in Fig. 9. The $\chi^2$ per degree of freedom is 1.24 in both fits. The difference between the Gaussian widths of the distribution is in fact compensated by different normalizations of the antiquark distributions obtained from the two fits.

## 5 The $\cos 2\phi$ asymmetry in unpolarized semi-inclusive DIS

Similar to the Drell–Yan process, in unpolarized semi-inclusive DIS

$$l(\ell) + N(P) \to l'(\ell') + h(P_h) + X(P_X)\,, \quad (51)$$

a $\cos 2\phi$ asymmetry can also occur, with $\phi$ the azimuthal angle of the final hadron $h$ with respect to the lepton plane, as shown in the reference frame in Fig. 10, which is commonly used in phenomenological analysis. Taking the intrinsic motion of quarks into account, the SIDIS cross section reads at leading order

$$\begin{aligned}\frac{\mathrm{d}\sigma}{\mathrm{d}x\,\mathrm{d}y\,\mathrm{d}z\,\mathrm{d}^2\boldsymbol{P}_T} &= \frac{2\pi\alpha_{\mathrm{em}}^2 s}{Q^4}\sum_q e_q^2\,x[1+(1-y)^2]\\ &\times \int \mathrm{d}^2\boldsymbol{k}_T \int \mathrm{d}^2\boldsymbol{p}_T\,\delta^2(\boldsymbol{P}_T - z\boldsymbol{k}_T - \boldsymbol{p}_T)\\ &\times f_1^q(x,\boldsymbol{k}_T^2)\,D_1^q(z,\boldsymbol{p}_T^2)\,,\end{aligned} \quad (52)$$

where $f_1^q(x,\boldsymbol{k}_T^2)$ is the unintegrated number density of quarks of flavor $q$ and $D_1^q(z,\boldsymbol{p}_T^2)$ is the transverse-momentum dependent fragmentation function of quark $q$ into the final hadron. Recall that the non-collinear factorization theorem for SIDIS has been proven by Ji, Ma, and Yuan [84] for $P_T \ll Q$.

The first measurement of the $\cos 2\phi$ asymmetry was performed by the EMC Collaboration at the energy

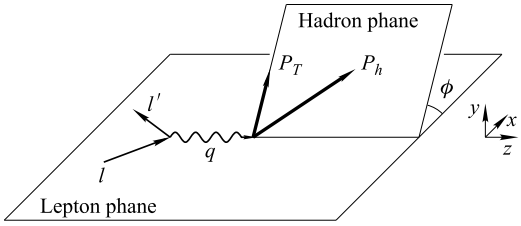


**Fig. 10** Kinematics in unpolarized semi-inclusive deep inelastic scattering.

$Q^2 > 4$ GeV$^2$, with $Q$ the virtuality of the intermediate photon. Later, the ZEUS Collaboration measured the asymmetry at $Q^2 > 180$ GeV$^2$. The $\cos 2\phi$ asymmetry of $\pi^+$ production in electroproduction on the proton was also searched by CLAS [113]. Several years ago, for the first time, the $\cos 2\phi$ asymmetries in a four-dimensional kinematic space ($x$, $y$, $z$, and $P_T$) for positively and negatively charged pions and kaons separately, as well as for unidentified hadrons, were measured by the HERMES Collaboration [112], with 27.6 GeV electrons and positrons scattered off unpolarized hydrogen and deuterium targets. An example of the HERMES measurement is given in Fig. 11, showing the asymmetries for $\pi^+$ and $\pi^-$ produced from the hydrogen and deuterium targets, respectively. The most recent data come from the COMPASS Collaboration [114], which obtained the $\cos 2\phi_h$ amplitude (together with the $\sin\phi_h$ and $\sin\phi_h$ modulations) binning the data separately in each of the relevant kinematic variables $x$, $z$ or $p_T^h$. The corresponding result on the $\cos 2\phi$ asymmetry binning in a three-dimensional grid of these three variables for positive and negative charged hadrons, measured with the CERN SPS muon beam at 160 GeV/c and a $^6$LiD target, is depicted in Fig. 12. The plots suggest strong kinematic dependencies of the asymmetries both for positive and negative hadrons. The data from different experimental measurements show that the magnitude of $\cos 2\phi$ asymmetry is substantial and can reach 10% at most. Moreover, the asymmetry is not suppressed at high energy, as can been seen from the ZEUS data.

### 5.1 Origins of the $\cos 2\phi$ asymmetry in SIDIS

In previous research, three possible mechanisms were developed to account for the $\cos 2\phi$ asymmetry in SIDIS. The first is the Cahn effect [115, 116], demonstrating that non-collinear kinematics at order $k_T^2/Q^2$ can generate the $\cos 2\phi$ angular dependence. The second is the high-order perturbative QCD effect [117–120], which shows that a certain azimuthal distribution of the final hadron can be aroused by gluon radiations from the struck quark or the fragmenting quark. The last mechanism is the Boer–Mulders function coupled to a specular fragmentation function, the so-called Collins function [121]. In the following, the features of the three mechanisms are outlined.

**Perturbative QCD effect.** At order $\alpha_s$, the following partonic processes participate in DIS:

$$\gamma^*(q) + q(k) \to q(k') + g\,,$$
$$\gamma^*(q) + q(k) \to g(k') + q\,,$$
$$\gamma^*(a) + g(k) \to q(k') + \bar{q}\,.$$

The effect is within the collinear picture, that is, the transverse momentum of the initial parton is not considered. However, each of the above processes can produce

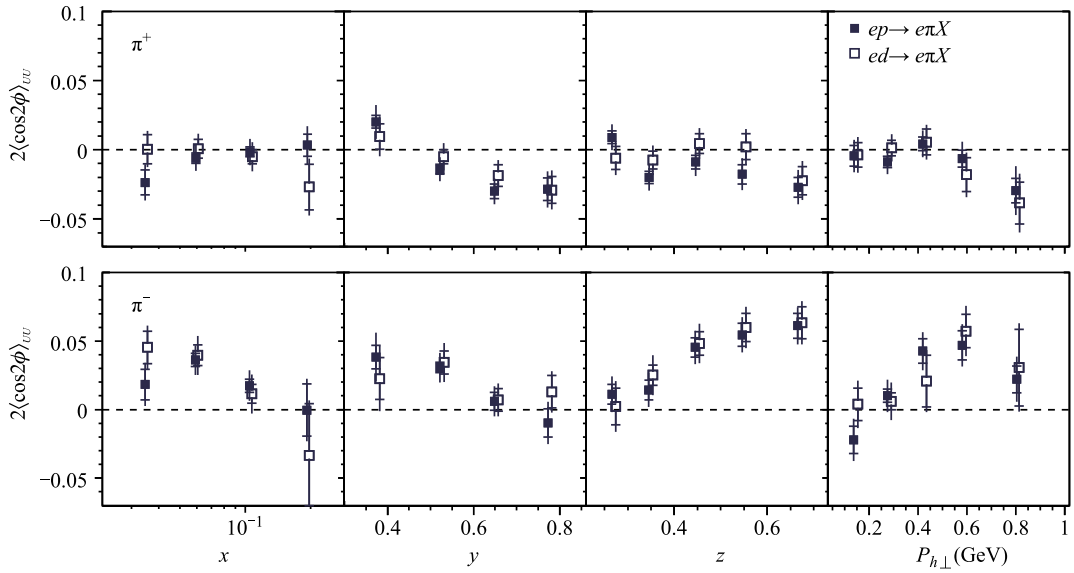


**Fig. 11** $\cos 2\phi$ amplitudes for positive (upper panels) and negative (lower panels) pions measured by the HERMES Collaboration [112]. Closed and open squares are for amplitudes extracted from hydrogen and deuterium targets, respectively.

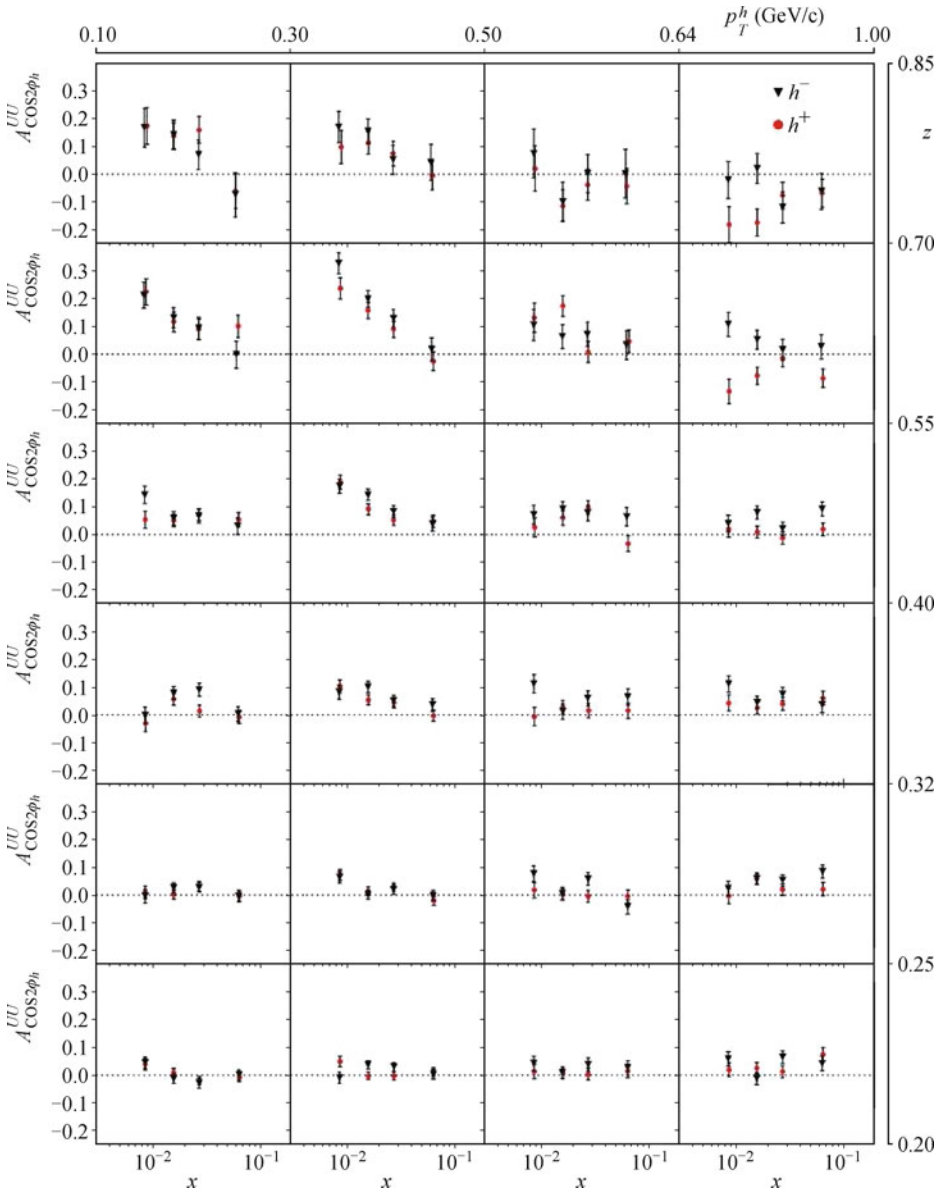


**Fig. 12** $A^{UU}_{\cos 2\phi_h}$ asymmetries for positive (*red points*) and negative (*black triangles*) hadrons as a function of $x$ for the different bins in $P_T^h$ (from left to right) and $z$ (from bottom to top) at COMPASS. The error bars show statistical uncertainties only.

a large transverse momentum for the final state parton. Such a contribution dominates the production of hadrons in a large $P_T$ region. The cross section at order $\mathcal{O}(\alpha_s)$ can be cast to [122]

$$\frac{\mathrm{d}^5\sigma^{(1)}}{\mathrm{d}x\,\mathrm{d}y\,\mathrm{d}z\,\mathrm{d}^2\boldsymbol{P}_T} = \frac{\alpha_{\rm em}^2\,e_q^2}{16\pi^2}\,\frac{y}{Q^4}\int_x^1 \frac{\mathrm{d}x'}{x'P_T^2+z_h^2(1-x')Q^2} \times \sum_{i,j} f_1^i\left(\frac{x}{x'}\right) L_{\mu\nu}\,M_{ij}^{\mu\nu}\,D_1^j\left(z+\frac{x'P_T^2}{z_h(1-x')Q^2}\right) \tag{53}$$

with $ij$ denoting the initial and final partons, $ij = qq, qg, gq$; and the parton variables $x'$ and $z'$ defined as

$$x' = \frac{Q^2}{2k\cdot q} = \frac{x}{\xi}, \quad z' = \frac{k\cdot k'}{k\cdot q} = \frac{z}{\zeta}, \tag{54}$$

similar to the hadronic variables $x$ and $z$.

The hard coefficients $L_{\mu\nu}\,M_{ij}^{\mu\nu}$ in Eq. (53) have the form [122, 123]

$$L_{\mu\nu}M_{qq}^{\mu\nu} = \frac{64\pi\alpha_s}{3}\,\frac{Q^2}{y^2}\left\{\cdots+4\,x'z'\,(1-y)\,\cos 2\phi\right\}, \tag{55}$$

$$L_{\mu\nu}M_{qg}^{\mu\nu} = \frac{64\pi\alpha_s}{3}\,\frac{Q^2}{y^2}\left\{\cdots+4x'(1-y)(1-z')\,\cos 2\phi\right\}, \tag{56}$$

$$L_{\mu\nu}M_{gq}^{\mu\nu} = 64\pi\alpha_s\frac{Q^2}{y^2}\Big\{\cdots + x'(1-x')(1-y)\cos 2\phi\Big\}. \quad (57)$$

Here the ellipses denote the angular independent and $\cos\phi$ dependent terms, respectively. Obviously the above equations contain the $\cos 2\phi$ contribution to the cross section, with $\phi$ the azimuthal angle of the fragmenting partons. Of course, in a collinear configuration, $\phi$ coincides with the azimuthal angle of the detected final hadron.

**The Cahn effect.** As shown a long time ago by Cahn [115, 116], the intrinsic transverse motion of partons can generate a $\cos 2\phi$ contribution to the unpolarized SIDIS cross section, which has the form

$$\frac{\mathrm{d}\sigma_{\mathrm{C}}}{\mathrm{d}x\,\mathrm{d}y\,\mathrm{d}z\,\mathrm{d}^2\boldsymbol{P}_T}\Big|_{\cos 2\phi} = \frac{8\pi\alpha_{\mathrm{em}}^2 s}{Q^4}\sum_q e_q^2\,x(1-y) \times \int \mathrm{d}^2\boldsymbol{k}_T \int \mathrm{d}^2\boldsymbol{p}_T\,\delta^2(\boldsymbol{P}_T - z\boldsymbol{k}_T - \boldsymbol{p}_T) \times \frac{2\,(\boldsymbol{k}_T\cdot\boldsymbol{h})^2 - \boldsymbol{k}_T^2}{Q^2}\,f_1^q(x,\boldsymbol{k}_T^2)\,D_1^q(z,\boldsymbol{p}_T^2)\,\cos 2\phi\,, \quad (58)$$

where $\boldsymbol{h} \equiv \boldsymbol{P}_T/P_T$.

**The Boer–Mulders effect.** Another $k_T$-dependent source of the $\cos 2\phi$ asymmetry involves the Boer–Mulders distribution $h_1^\perp$ coupled to the Collins fragmentation function $H_1^\perp$, which is also chirally odd and describes the fragmentation of transversely polarized quarks into unpolarized hadrons. The explicit expression of this contribution to the cross section is [15]

$$\frac{\mathrm{d}\sigma_{\mathrm{BM}}}{\mathrm{d}x\,\mathrm{d}y\,\mathrm{d}z\,\mathrm{d}^2\boldsymbol{P}_T}\Big|_{\cos 2\phi} = \frac{4\pi\alpha_{\mathrm{em}}^2 s}{Q^4}\sum_q e_q^2\,x(1-y) \times \int \mathrm{d}^2\boldsymbol{k}_T \int \mathrm{d}^2\boldsymbol{p}_T\,\delta^2(\boldsymbol{P}_T - z\boldsymbol{k}_T - \boldsymbol{p}_T) \times \frac{2\,\boldsymbol{h}\cdot\boldsymbol{k}_T\,\boldsymbol{h}\cdot\boldsymbol{p}_T - \boldsymbol{k}_T\cdot\boldsymbol{p}_T}{zMM_h} \times h_1^{\perp q}(x,\boldsymbol{k}_T^2)\,H_1^{\perp a}(z,\boldsymbol{p}_T^2)\,\cos 2\phi\,, \quad (59)$$

Although both the Boer–Mulders and Cahn effects involve transverse kinematics, there are two major differences between them. The first difference is that the Boer–Mulders effect generates a leading-twist contribution; hence, it is not suppressed by inverse powers of $Q$. On the contrary, the contribution from the Cahn effect is of the order $k_T^2/Q^2$; hence, in terms of kinematics it is a higher twist effect. The second difference is that for the Cahn effect, the initial and final partons are unpolarized, whereas for the Boer–Mulders effect, the partons are transversely polarized. Therefore, similar to the Drell–Yan process, SIDIS also provides an opportunity to probe the transverse polarization of quarks inside an unpolarized nucleon by measuring the $\cos 2\phi$ azimuthal asymmetry.

### 5.2 Phenomenological analysis on the $\cos 2\phi$ asymmetry in SIDIS

The last decade has seen a considerable number of phenomenological studies [109, 124–132] on the unpolarized leptoproduction at EMC, ZEUS, HERMES, JLab, and COMPASS based upon one or more of the three mechanisms. In the analysis of Ref. [124], the perturbative contribution and the Cahn effect were included, whereas the Boer–Mulders effect was not considered. In Refs. [125, 126] the contribution from the Boer–Mulders effect to the $\cos 2\phi$ asymmetry of $\pi^+$ at the kinematics domain of HERMES was estimated using a spectator model from Refs. [33, 34]. The Boer–Mulders effect combined with the contribution from the Cahn effect on the $\cos 2\phi$ asymmetry of pions at ZEUS, EMC, HERMES, and COMPASS is also evaluated in Ref. [127], where a spectator model [87] for $h_1^\perp$ adjusted on Drell–Yan data was used. Furthermore, in that work, the asymmetries were calculated according to their experimental definition (which incorporates a cutoff on the transverse momentum of the final hadron). The analysis demonstrates that both the Boer–Mulders effect and the Cahn effect contribute sizable asymmetry, around several percent. The asymmetry estimated at ZEUS using the calculation in Ref. [127] is depicted in Fig. 13, showing that the agreement is rather good for low values of the $P_T$ cutoff (up to 0.5 GeV). In Ref. [133], the $\cos 2\phi$ asymmetries at the kinematic regimes of ZEUS, HERMES, and JLab were revisited, using the Boer–Mulders function from a fit [96] to the $pd$ Drell–Yan.

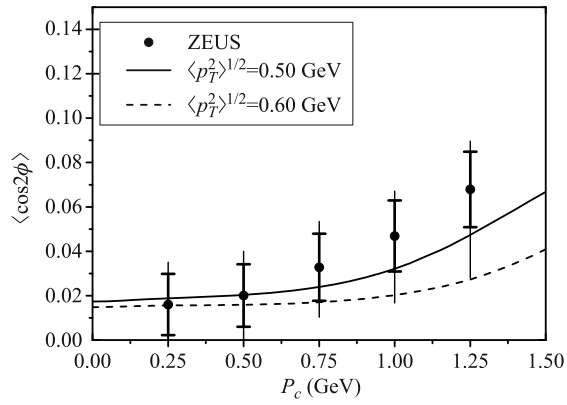


**Fig. 13** The SIDIS $\cos 2\phi$ azimuthal asymmetry as a function of the cutoff $P_c$ in the ZEUS domain compared with the ZEUS Data [134]. The dotted curve is the leading-twist Boer–Mulders contribution, the dashed curve is the higher-twist term, the solid curve is the sum of the two contributions.

A more comprehensive phenomenological study on the $\cos 2\phi$ asymmetry for charged pions in unpolarized SIDIS was conducted in Ref. [128], in which the authors not only considered the Boer–Mulders effect and the Cahn effect, but also included the perturbative QCD effect. In order to estimate the contribution from the Boer–Mulders function, they applied the impact-parameter approach [57, 58, 60, 135] to connect the anomalous tensor magnetic moment of quarks $\kappa_T^q$ and the Boer–Mulders function in a model dependent way: $h_1^{\perp q} \sim \kappa_T$. The Boer–Mulders function is finally related to the Sivers function by assuming the sizes of the two distributions are alike, up to a scale factor $\frac{\kappa_T}{\kappa}$:

$$h_1^{\perp q} = \frac{\kappa_T}{\kappa} f_{1T}^{\perp,q}. \tag{60}$$

It is found that the perturbative contribution dominates the asymmetry at ZEUS where the average $Q^2$ value is around $\langle Q^2 \rangle = 750$ GeV$^2$), whereas it is almost negligible at the kinematics of HEMERS, JLab, and COMPASS (except large $P_T$ region at COMPASS). Another interesting observation in Ref. [128] is that the difference between $\langle \cos 2\phi \rangle^{\pi^+}$ and $\langle \cos 2\phi \rangle^{\pi^-}$ can be viewed as a clear signature of the Boer–Mulders effect.

In a new analysis on the $\cos 2\phi$ asymmetry presented in Ref. [129], the impact of the kinematical constraints of parton transverse momenta is considered. By requiring the parton energy to be smaller than the energy of its parent hadron and preventing the parton to move backwards relative to its parent hadron, an upper bound for the range of allowed values of $k_T$ is determined:

$$k_T^2 \leqslant (2-x)(1-x)Q^2, \quad 0 < x < 1, \tag{61}$$

$$k_T^2 \leqslant \frac{x(1-x)}{(1-2x)^2} Q^2, \quad x < 0.5. \tag{62}$$

Imposing the above constraints significantly reduces the Cahn effect, as can be seen in the upper panels of Fig. 14. This is because the constraints in Eqs. (61) and (62) effectively reduce the Gaussian width $\langle k_T^2 \rangle$. On the contrary, the lower panels of Fig. 14 show that the Boer–Mulders contribution is not sensitive to the $k_T$ constraints.

### 5.3 Extraction of the quark Boer–Mulders function from SIDIS data

A recent development in the phenomenology of unpolarized SIDIS is the extraction of the quark Boer–Mulders function using the $\cos 2\phi$ asymmetry data collected by HERMES and COMPASS, as the contribution of the Boer–Mulders effect is substantial. To date two different fits [109, 131] have been performed, using two different data sets.

#### *5.3.1 Parameterization in Ref. [109]*

In an earlier extraction conducted in Ref. [109], the preliminary data from the HERMES [136] and the COMPASS [137, 138] collaborations are used. The limited

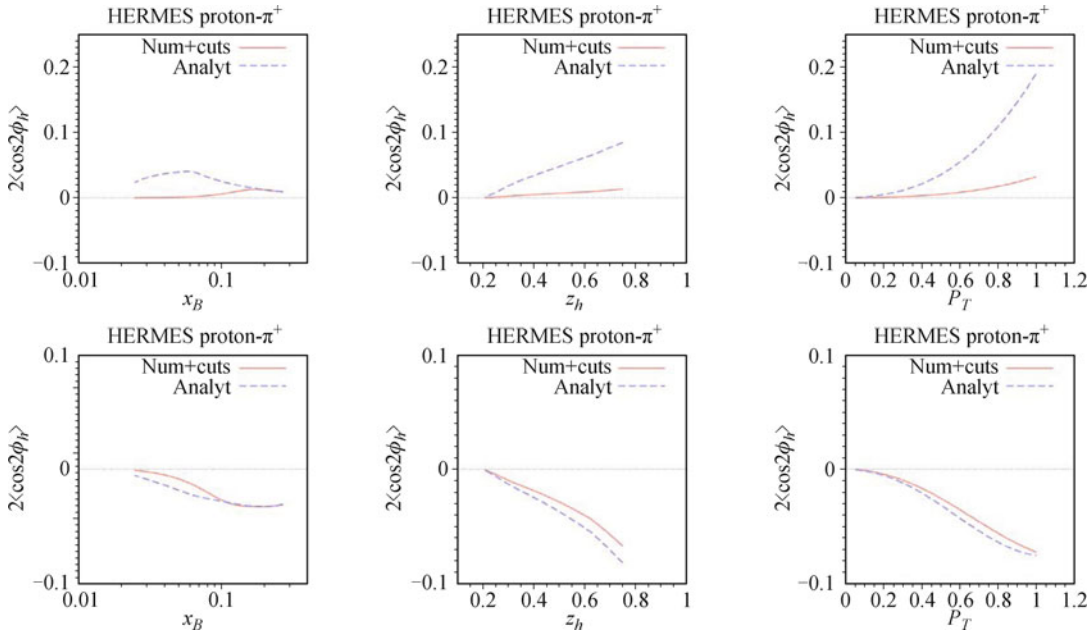


**Fig. 14** Effect of kinematical constraints on the $\cos 2\phi$ asymmetries in SIDIS analyzed in Ref. [129]. The upper panels and lower panels show the twist-4 Cahn contribution and twist-2 Boer–Mulders contribution to the $\langle \cos 2\phi_h \rangle$ azimuthal modulation for $\pi^+$ production at HERMES as a function of $x$ (left plot), $z$ (central plot) and $P_T$ (right plot), respectively The dashed and solid lines show the results without and with the kinematical cuts, respectively.

availability of data at that time required the author to simply take $h_1^\perp$ to be proportional to the Sivers function $f_{1T}^\perp$,

$$h_1^{\perp q}(x,k_T^2) = \lambda_q\, f_{1T}^{\perp q}(x,k_T^2) = \lambda_q\, \rho_q(x)\, \eta(k_T)\, f_1^q(x,\boldsymbol{k}_T^2)\,, \tag{63}$$

where

$$\rho_q(x) = A_q\, x^{a_q}(1-x)^{b_q}\, \frac{(a_q+b_q)^{(a_q+b_q)}}{a_q^{a_q} b_q^{b_q}}, \tag{64}$$

$$\eta(k_T) = \sqrt{2e}\, \frac{M_P}{M_1}\, \mathrm{e}^{-k_T^2/M_1^2}. \tag{65}$$

and $A_q$, $a_q$, $b_q$, and $M_1$ are known parameters for the quark Sivers functions fixed in Ref. [139]. The only free parameter to be fitted is the coefficient $\lambda_q$. Therefore, in this fit the $x$ and $k_T$ dependence of the Boer–Mulders function follows those of the Sivers function. For the Collins function coupled to the Boer–Mulders function, the parametrization of Ref. [140] is adopted, based on a combined analysis of SIDIS and $e^+e^-$ data. In addition, in the extraction, a Gaussian transverse momentum distribution is assumed for all the distribution/fragmentation functions. Two fitted results are obtained:

$$\lambda_u = 2.0 \pm 0.1\,, \quad \lambda_d = -1.111 \pm 0.001 \quad \text{(Fit 1)}\,,$$
$$\lambda_u = 2.1 \pm 0.1\,, \quad \lambda_d = -1.111 \pm 0.001 \quad \text{(Fit 2)}\,,$$

corresponding to two different choices for the average transverse momenta for the unpolarized distribution and fragmentation functions.

### 5.3.2 *Parameterization in Ref. [131]*

The HERMES and COMPASS Collaborations have recently performed measurements on SIDIS to provide multidimensional data in bins of $x_B, z_h, Q^2$, and $P_T$ for the azimuthal asymmetries [112, 114], which allows the extraction of the quark Boer–Mulders functions in a more comprehensive way. Particularly, it is possible to carry out the analysis up to an order of $\mathcal{O}(1/Q)$. At this order, only the Boer–Mulders effect contributes to the $\cos 2\phi$ asymmetry, since the Cahn effect for the $\cos 2\phi$ modulation is a twist-4 effect and is $1/Q^2$ suppressed. However, at the order of $\mathcal{O}(1/Q)$, both the Boer–Mulders and Cahn effects give rise to the $\cos\phi$ asymmetry [131]:

$$F_{UU}^{\cos\phi}\Big|_{\text{Cahn}} = -2\sum_q e_q^2 x \int \mathrm{d}^2\boldsymbol{k}_T\, \frac{(\boldsymbol{k}_T\cdot\boldsymbol{h})}{Q} \times f_q(x,\boldsymbol{k}_T^2) D_q(z,\boldsymbol{p}_T^2), \tag{66}$$

$$F_{UU}^{\cos\phi}\Big|_{\text{BM}} = \sum_q e_q^2 x \int \mathrm{d}^2\boldsymbol{k}_T\, \frac{k_T}{Q}\frac{P_T - z(\boldsymbol{k}_T\cdot\boldsymbol{h})}{k_T} \times \Delta f_{q^\uparrow/p}(x,\boldsymbol{k}_T^2)\Delta D_{h/q^\uparrow}(z,\boldsymbol{p}_T^2). \tag{67}$$

Here

$$D_{h/q^\uparrow}(z,\boldsymbol{p}_T^2) = \frac{2P_T}{zM_h} H_1^{\perp q}(z,p_T^2) \tag{68}$$

is another notation for the Collins function [30]. For this reason, the data of $\cos\phi$ asymmetry were also included in the fit of Ref. [131].

The extraction is performed by using the following parametrization form for the Boer–Mulders functions:

$$\Delta f_{q^\uparrow/p}(x,k_T) = \Delta f_{q^\uparrow/p}(x)\, \sqrt{2e}\, \frac{k_T}{M_{\text{BM}}}\, \frac{\mathrm{e}^{-k_T^2/\langle k_\perp^2\rangle_{\text{BM}}}}{\pi\langle k_\perp^2\rangle}, \tag{69}$$

with

$$\Delta f_{q^\uparrow/p}(x) = N_q\, \frac{(\alpha_q+\beta_q)^{\alpha_q+\beta_q}}{\alpha_q^{\alpha_q}\beta_q^{\beta_q}}\, x^{\alpha_q}(1-x)^{\beta_q}\, f_{q/p}(x), \tag{70}$$

$$\langle k_T^2\rangle_{\text{BM}} = \frac{\langle k_T^2\rangle\, M^2{}_{\text{BM}}}{\langle k_T^2\rangle + M^2{}_{\text{BM}}}, \tag{71}$$

where $N_q$, $\alpha_q$, $\beta_q$, and $M_{\text{BM}}$ are free parameters in the model. In addition, the mean transverse momentum of the final state quark is assumed to be $z$-dependent:

$$\langle p_T^2\rangle = A + Bz^2\,; \tag{72}$$

therefore, (defining $\langle k_T^2\rangle = C$)

$$\langle P_T^2\rangle = \langle p_T^2\rangle + z^2\langle k_T^2\rangle = A + (B+C)z^2\,, \tag{73}$$

with $A$, $B$, and $C$ the three additional constant parameters to be determined by the fit. In the practical extraction of Ref. [131], two parameters are fixed as $\alpha_q = \beta_q = 0$, that is, $\Delta f_{q^\uparrow/p}(x)$ is proportional to $f_{q/p}(x)$. The fitted values of the remaining parameters are given in Tables 1 and 2 of [131] for the HERMES and COMPASS data, respectively. As an example, the best fit curves [131] for $\cos 2\phi$ asymmetry obtained by fitting the COMPASS data are shown in Fig. 15. Although the Cahn effect is a higher twist effect, quantitative studies [127–129] show that it has been found to be significant at the kinematics region in which $Q$ is not large. Therefore, the Cahn effect may strongly affect the extraction [131] of the Boer–Mulders function from SIDIS data.

## 6 Prospects and summary

In summary, nowadays it has been widely recognized that the Boer–Mulders function plays an important role in describing the spin and transverse structure of unpolarized hadrons. As a T-odd and TMD distribution, the Boer–

Mulders function manifests a unique correlation between the transverse spin and transverse momentum of quarks; thus, its investigation can provide an enhanced understanding of QCD dynamics, such as the color gauge invariance of TMD distributions. Selected basic features of the Boer–Mulders function have been explored in a considerable number of theoretical and experimental studies performed during the last decade. Although the calculation of TMD distributions from the first principles of QCD is not possible, several phenomenological models inspired by QCD were applied to calculate the quark Boer–Mulders functions of the nucleon and the pion, starting from their operator definitions. An intriguing result is that the signs of the Boer–Mulders functions of the up and down quarks are both negative (in SIDIS), which is predicted by almost all models. Besides, the first $k_T$-moment of the quark Boer–Mulders function timed with $x$ is found to be sizable, about several percent, although the magnitudes are quantitatively different in different models. The same-sign feature is also confirmed in the extractions of the Boer–Mulders function from the $\cos 2\phi$ asymmetries in Drell–Yan data as well as the SIDIS data.

Meanwhile, more efforts are required to achieve an improved understanding of $h_1^\perp$. An open question is the TMD evolution effect of $h_1^\perp$, which has not been considered in previous phenomenological studies [141].

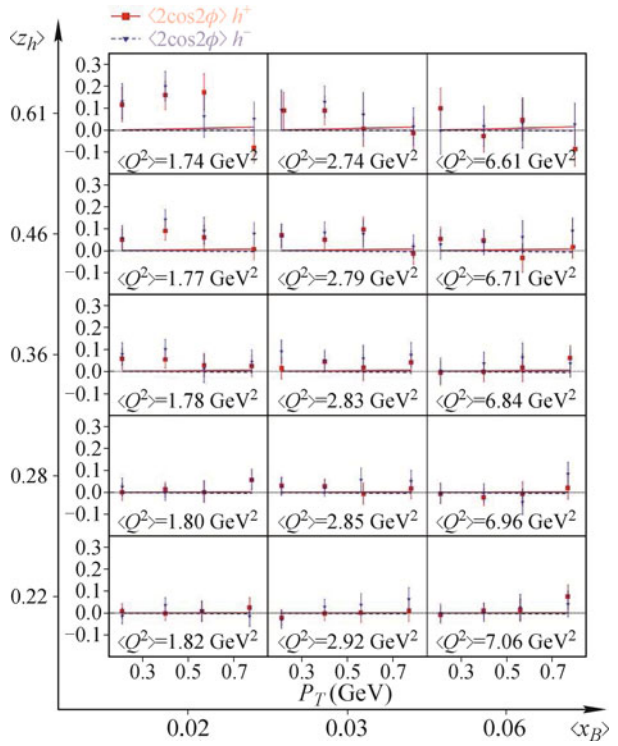


**Fig. 15** Best fit curves [131] for $\langle \cos 2\phi \rangle$ obtained by fitting COMPASS data on $\langle \cos \phi \rangle$ and $\langle \cos 2\phi \rangle$. The Cahn effect in $\langle \cos 2\phi \rangle$ has been set to zero.

**Table 4** Existing and proposed experiments that are capable to measure the $\cos 2\phi$ asymmetry in the unpolarized Drell–Yan process.

| Experiment | Particles | Energy | $\sqrt{s}$ (GeV) |
|---|---|---|---|
| COMPASS | $\pi^\pm + p$ | 160 | 17.4 |
| COMPASS (low mass) | $\pi^\pm + p$ | 160 | 17.4 |
| SeaQuest | $p + p$ | 120 | 15 |
| PANDA | $\bar{p} + p$ | 15 | 5.5 |
| J-PARC | $p + p$ | 50 | 10 |
| NICA | $p + p$ | collider | 20 |
| PAX | $\bar{p} + p$ | collider | 14 |
| AFTER | $p + p$ | 7000 | 115 |
| RHIC | $p + p$ | 250 | 22 |

However, as shown in the cases of the Sivers function [142–145] and the transversity [13, 144], the effect of TMD evolution can be large and can significantly alter the corresponding spin asymmetries. Therefore, it is necessary to study the TMD evolution of the Boer–Mulders function, as well as the impact of the effect of the evolution on the azimuthal asymmetries in unpolarized Drell–Yan/SIDIS processes. This is important for the global fit of $h_1^\perp$ using the data from different experimental configurations. Besides, the precision measurement of the $\cos 2\phi$ asymmetry in the unpolarized Drell–Yan or SIDIS process will be pursued in active scientific programs in existing or planned experimental facilities. The performance of the unpolarized Drell–Yan is feasible in a number of experiments [18, 147] spanning a wide range of energies, as shown in Table 4. Particularly, the $\pi + p$ Drell–Yan program at COMPASS-II is able to not only probe the Boer–Mulders of the nucleon, but also that of the pion. In the case of the SIDIS process, the precision measurement of the Boer–Mulders function at the valence region is promising once the 12 GeV upgrade at JLab [148] is complete. Moreover, at the planned Electron Ion Collider (EIC) [149, 150], on the one hand, the Boer–Mulders function for sea quarks may be probed; on the other hand, the experimental cuts and the $Q^2$ range could be easily adjusted to choose the desirable kinematic region. Future theoretical and experimental studies are definitely expected to provide great opportunities to clarify the Boer–Mulders function of different quark flavors and unravel the spin structure of unpolarized hadrons at considerable precision.

**Acknowledgements** Z. L. thanks Vincenzo Barone, Bo-Qiang Ma, and Ivan Schmidt on the collaborations valuable discussion on some of the topics in the paper. This work was partially supported by the National Natural Science Foundation of China (Grants Nos. 11575043, 11005018, and 11120101004), and the Qing Lan Project.

## References


1. B. W. Filippone and X. D. Ji, The spin structure of the nucleon, *Adv. Nucl. Phys.* 26, 1 (2001)
2. V. Barone, A. Drago, and P. G. Ratcliffe, Transverse polarisation of quarks in hadrons, *Phys. Rep.* 359(1–2), 1 (2002), arXiv: hep-ph/0104283
3. C. A. Aidala, S. D. Bass, D. Hasch, and G. K. Mallot, The spin structure of the nucleon, *Rev. Mod. Phys.* 85(2), 655 (2013), arXiv: 1209.2803
4. S. J. Brodsky, M. Burkardt, and I. Schmidt, QCD constraints on the shape of polarized quark and gluon distributions, *Nucl. Phys. B* 441(1–2), 197 (1995)
5. B. Q. Ma, The $x$-dependent helicity distributions for valence quarks in nucleons, *Phys. Lett. B* 375(1–4), 320 (1996)
6. C. Bourrely, J. Soffer, and F. Buccella, A statistical approach for polarized parton distributions, *Eur. Phys. J. C* 23(3), 487 (2002)
7. T. Gehrmann and W. J. Stirling, Polarized parton distributions in the nucleon, *Phys. Rev. D* 53(11), 6100 (1996)
8. M. Glück, E. Reya, M. Stratmann, and W. Vogelsang, Models for the polarized parton distributions of the nucleon, *Phys. Rev. D* 63(9), 094005 (2001)
9. M. Hirai, S. Kumano, and N. Saito, Determination of polarized parton distribution functions with recent data on polarization asymmetries, *Phys. Rev. D* 74(1), 014015 (2006)
10. D. de Florian, R. Sassot, M. Stratmann, and W. Vogelsang, Global analysis of helicity parton densities and their uncertainties, *Phys. Rev. Lett.* 101(7), 072001 (2008)
11. E. Leader, A. V. Sidorov, and D. B. Stamenov, Determination of polarized parton densities from a QCD analysis of inclusive and semi-inclusive deep inelastic scattering data, *Phys. Rev. D* 82(11), 114018 (2010)
12. M. Anselmino, M. Boglione, U. D'Alesio, S. Melis, F. Murgia, and A. Prokudin, Simultaneous extraction of transversity and Collins functions from new semi-inclusive deep inelastic scattering and $e^+e^-$ data, *Phys. Rev. D* 87(9), 094019 (2013), arXiv: 1303.3822 [hep-ph]
13. Z. B. Kang, A. Prokudin, P. Sun, and F. Yuan, Extraction of quark transversity distribution and collins fragmentation functions with QCD evolution, arXiv: 1505.05589 [hep-ph]
14. P. J. Mulders and R. D. Tangerman, The complete tree-level result up to order $1/Q$ for polarized deep-inelastic leptoproduction, *Nucl. Phys. B* 461(1–2), 197 (1996) [Erratum: *Nucl. Phys. B* 484, 538 (1997)]
15. D. Boer and P. J. Mulders, Time-reversal odd distribution functions in leptoproduction, *Phys. Rev. D* 57(9), 5780 (1998), arXiv: hep-ph/9711485
16. K. Goeke, A. Metz, and M. Schlegel, Parameterization of the quark-quark correlator of a spin-1/2 hadron, *Phys. Lett. B* 618(1–4), 90 (2005), arXiv: hep-ph/0504130
17. A. Bacchetta, M. Diehl, K. Goeke, A. Metz, P. J. Mulders, and M. Schlegel, Semi-inclusive deep inelastic scattering at small transverse momentum, *J. High Energy Phys.* 0702, 093 (2007), arXiv: hep-ph/0611265
18. V. Barone, F. Bradamante, and A. Martin, Transverse-spin and transverse-momentum effects in high-energy processes, *Prog. Part. Nucl. Phys.* 65(2), 267 (2010), arXiv: 1011.0909 [hep-ph]
19. K. B. Chen, S. Y. Wei, and Z. T. Liang, Three dimensional imaging of the nucleon and semi-inclusive high energy reactions, arXiv: 1506.07302 [hep-ph]
20. D. W. Sivers, Single-spin production asymmetries from the hard scattering of pointlike constituents, *Phys. Rev. D* 41(1), 83 (1990)
21. D. Sivers, Hard-scattering scaling laws for single-spin production asymmetries, *Phys. Rev. D* 43(1), 261 (1991)
22. J. C. Collins, Fragmentation of transversely polarized quarks probed in transverse momentum distributions, *Nucl. Phys. B* 396(1), 161 (1993), arXiv: hep-ph/9208213
23. S. J. Brodsky, D. S. Hwang, and I. Schmidt, Final-state interactions and single-spin asymmetries in semi-inclusive deep inelastic scattering, *Phys. Lett. B* 530(1–4), 99 (2002)
24. S. J. Brodsky, D. S. Hwang, and I. Schmidt, Initial-state interactions and single-spin asymmetries in Drell–Yan processes, *Nucl. Phys. B* 642(1–2), 344 (2002), arXiv: hep-ph/0206259
25. J. C. Collins, Leading-twist single-transverse-spin asymmetries: Drell–Yan and deep-inelastic scattering, *Phys. Lett. B* 536(1–2), 43 (2002), arXiv: hep-ph/0204004
26. X. Ji and F. Yuan, Parton distributions in light-cone gauge: Where are the final-state interactions– *Phys. Lett. B* 543(1–2), 66 (2002), arXiv: hep-ph/0206057
27. A. V. Belitsky, X. Ji, and F. Yuan, Final state interactions and gauge invariant parton distributions, *Nucl. Phys. B* 656(1–2), 165 (2003), arXiv: hep-ph/0208038
28. D. Boer, P. J. Mulders, and F. Pijlman, Universality of $T$-odd effects in single spin and azimuthal asymmetries, *Nucl. Phys. B* 667(1–2), 201 (2003), arXiv: hep-ph/0303034
29. A. Bacchetta, U. D'Alesio, M. Diehl, and C. A. Miller, Single-spin asymmetries: The Trento conventions, *Phys. Rev. D* 70(11), 117504 (2004), arXiv: hep-ph/0410050
30. M. Anselmino, U. D'Alesio, and F. Murgia, Transverse single spin asymmetries in Drell–Yan processes, *Phys. Rev. D* 67(7), 074010 (2003), arXiv: hep-ph/0210371
31. R. L. Jaffe, Spin, twist and hadron structure in deep inelastic processes, *Lect. Notes Phys.* 496, 178 (1997), arXiv: hep-ph/9602236
32. D. Boer, S. J. Brodsky, and D. S. Hwang, Initial-state interactions in the unpolarized Drell–Yan process, *Phys. Rev. D* 67(5), 054003 (2003), arXiv: hep-ph/0211110

33. L. P. Gamberg, G. R. Goldstein, and K. A. Oganessyan, Novel transversity properties in semi-inclusive deep inelastic scattering, *Phys. Rev. D* 67(7), 071504 (2003), arXiv: hep-ph/0301018
34. G. R. Goldstein and L. Gamberg, Transversity and Meson photoproduction, arXiv: hep-ph/0209085
35. A. Bacchetta, A. Schäfer, and J. J. Yang, Sivers function in a spectator model with axial-vector diquarks, *Phys. Lett. B* 578(1–2), 109 (2004), arXiv: hep-ph/0309246
36. P. V. Pobylitsa, Transverse-momentum dependent parton distributions in large-$N_c$ QCD, arXiv: hep-ph/0301236
37. Z. Lu, B. Q. Ma, and I. Schmidt, Flavor separation of the Boer–Mulders function from unpolarized $\pi$-p and $\pi$-D Drell–Yan processes, *Phys. Lett. B* 639, 494 (2006), arXiv: hep-ph/0702006 [hep-ph]
38. L. P. Gamberg, G. R. Goldstein, and M. Schlegel, Transverse quark spin effects and the flavor dependence of the Boer–Mulders function, *Phys. Rev. D* 77(9), 094016 (2008), arXiv: 0708.0324 [hep-ph]
39. M. Burkardt and B. Hannafious, Are all Boer–Mulders functions alike? *Phys. Lett. B* 658(4), 130 (2008), arXiv: 0705.1573 [hep-ph]
40. A. Bacchetta, F. Conti, and M. Radici, Transverse-momentum distributions in a diquark spectator model, *Phys. Rev. D* 78(7), 074010 (2008), arXiv: 0807.0323 [hep-ph]
41. F. Yuan, Sivers function in the MIT bag model, *Phys. Lett. B* 575(1–2), 45 (2003), arXiv: hep-ph/0308157
42. A. Courtoy, S. Scopetta, and V. Vento, Analyzing the Boer–Mulders function within different quark models, *Phys. Rev. D* 80(7), 074032 (2009), arXiv: 0909.1404 [hep-ph]
43. Z. Lü and B. Q. Ma, Sivers function in light-cone quark model and azimuthal spin asymmetries in pion electroproduction, *Nucl. Phys. A* 741, 200 (2004), arXiv: hep-ph/0406171
44. Z. Lü and B. Q. Ma, Nonzero transversity distribution of the pion in a quark-spectator-antiquark model, *Phys. Rev. D* 70(9), 094044 (2004), arXiv: hep-ph/0411043
45. S. Meissner, A. Metz, M. Schlegel, and K. Goeke, Generalized parton correlation functions for a spin-0 hadron, *J. High Energy Phys.* 0808, 038 (2008), arXiv: 0805.3165 [hep-ph]
46. L. Gamberg and M. Schlegel, Final state interactions and the transverse structure of the pion using non-perturbative eikonal methods, *Phys. Lett. B* 685(1), 95 (2010), arXiv: 0911.1964 [hep-ph]
47. B. Pasquini and F. Yuan, Sivers and Boer–Mulders functions in light-cone quark models, *Phys. Rev. D* 81(11), 114013 (2010), arXiv: 1001.5398 [hep-ph]
48. Z. Lu, B. Q. Ma, and J. Zhu, Boer–Mulders function of the pion in the MIT bag model, *Phys. Rev. D* 86(9), 094023 (2012), arXiv: 1211.1745 [hep-ph]
49. R. Jakob, P. J. Mulders, and J. Rodrigues, Modelling quark distribution and fragmentation functions, *Nucl. Phys. A* 626(4), 937 (1997), arXiv: hep-ph/9704335
50. S. J. Brodsky, D. S. Hwang, B. Q. Ma, and I. Schmidt, Light-cone representation of the spin and orbital angular momentum of relativistic composite systems, *Nucl. Phys. B* 593(1–2), 311 (2001), arXiv: hep-th/0003082
51. J. She, J. Zhu, and B. Q. Ma, Pretzelosity $h_{1T}^{\perp}$ and quark orbital angular momentum, *Phys. Rev. D* 79(5), 054008 (2009), arXiv: 0902.3718 [hep-ph]
52. Z. Lu and I. Schmidt, Connection between the Sivers function and the anomalous magnetic moment, *Phys. Rev. D* 75(7), 073008 (2007), arXiv: hep-ph/0611158
53. S. J. Brodsky, H. C. Pauli, and S. S. Pinsky, Quantum chromodynamics and other field theories on the light cone, *Phys. Rep.* 301(4–6), 299 (1998), arXiv: hep-ph/9705477
54. M. Gockeler, et al. (QCDSF and UKQCD Collaborations), Transverse spin structure of the nucleon from lattice-QCD simulations, *Phys. Rev. Lett.* 98(22), 222001 (2007), arXiv: hep-lat/0612032
55. B. Pasquini and S. Boffi, Nucleon spin densities in a light-front constituent quark model, *Phys. Lett. B* 653(1), 23 (2007), arXiv: 0705.4345 [hep-ph]
56. B. Pasquini and P. Schweitzer, Pion transverse momentum dependent parton distributions in a light-front constituent approach, and the Boer–Mulders effect in the pion-induced Drell–Yan process, *Phys. Rev. D* 90(1), 014050 (2014), arXiv: 1406.2056 [hep-ph]
57. M. Diehl and P. Hagler, Spin densities in the transverse plane and generalized transversity distributions, *Eur. Phys. J. C* 44(1), 87 (2005), arXiv: hep-ph/0504175
58. M. Burkardt, Transverse deformation of parton distributions and transversity decomposition of angular momentum, *Phys. Rev. D* 72(9), 094020 (2005), arXiv: hep-ph/0505189
59. M. Burkardt, Impact parameter dependent parton distributions and transverse single spin asymmetries, *Phys. Rev. D* 66(11), 114005 (2002), arXiv: hep-ph/0209179
60. M. Burkardt, Chromodynamic lensing and transverse single spin asymmetries, *Nucl. Phys. A* 735(1–2), 185 (2004)
61. M. Burkardt and D. S. Hwang, Sivers effect and generalized parton distributions in impact parameter space, *Phys. Rev. D* 69(7), 074032 (2004), arXiv: hep-ph/0309072
62. S. Meissner, A. Metz, and K. Goeke, Relations between generalized and transverse momentum dependent parton distributions, *Phys. Rev. D* 76, 034002 (2007), arXiv: hep-ph/0703176 [hep-ph]
63. S. Meissner, A. Metz, and M. Schlegel, Generalized parton correlation functions for a spin-1/2 hadron, *J. High Energy Phys.* 0908, 056 (2009), arXiv: 0906.5323 [hep-ph]
64. S. D. Drell and T. M. Yan, Massive lepton-pair production in hadron-hadron collisions at high energies, *Phys. Rev. Lett.* 25(5), 316 (1970) [Erratum: *Phys. Rev. Lett.* 25, 902 (1970)]
65. S. D. Drell and T. M. Yan, Partons and their applications at high energies, *Ann. Phys.* 66(2), 578 (1971) [*Ann. Phys.* 281, 450 (2000)]

66. J. C. Peng and J. W. Qiu, Novel phenomenology of parton distributions from the Drell–Yan process, *Prog. Part. Nucl. Phys.* 76, 43 (2014), arXiv: 1401.0934 [hep-ph]
67. J. C. Collins and D. E. Soper, Angular distribution of dileptons in high-energy hadron collisions, *Phys. Rev. D* 16(7), 2219 (1977)
68. K. Gottfried and J. D. Jackson, On the connection between production mechanism and decay of resonances at high energies, *Nuovo Cim.* 33(2), 309 (1964)
69. C. S. Lam and W. K. Tung, Systematic approach to inclusive lepton pair production in hadronic collisions, *Phys. Rev. D* 18(7), 2447 (1978)
70. S. Falciano, et al. (NA10 Collaboration), Angular distributions of muon pairs produced by 194 GeV/c negative pions, *Z. Phys. C* 31(4), 513 (1986)
71. M. Guanziroli, et al. (NA10 Collaboration), Angular distributions of muon pairs produced by negative pions on deuterium and tungsten, *Z. Phys. C* 37(4), 545 (1988)
72. J. S. Conway, C. E. Adolphsen, J. P. Alexander, K. J. Anderson, J. G. Heinrich, J. E. Pilcher, A. Possoz, E. I. Rosenberg, C. Biino, J. F. Greenhalgh, W. C. Louis, K. T. McDonald, S. Palestini, F. C. Shoemaker, and A. J. S. Smith, Experimental study of muon pairs produced by 252 GeV pions on tungsten, *Phys. Rev. D* 39(1), 92 (1989)
73. J. C. Collins, Simple prediction of quantum chromodynamics for angular distribution of dileptons in hadron collisions, *Phys. Rev. Lett.* 42(5), 291 (1979)
74. A. Brandenburg, O. Nachtmann, and E. Mirkes, Spin effects and factorization in the Drell–Yan process, *Z. Phys. C* 60(4), 697 (1993)
75. D. Boer and W. Vogelsang, Drell–Yan lepton angular distribution at small transverse momentum, *Phys. Rev. D* 74(1), 014004 (2006), arXiv: hep-ph/0604177
76. M. Blažek, M. Biyajima, and N. Suzuki, Angular distribution of muon pairs produced by negative pions on deuterium and tungsten in terms of coherent states, *Z. Phys. C* 43(3), 447 (1989)
77. A. Brandenburg, S. J. Brodsky, V. V. Khoze, and D. Müller, Angular distributions in the Drell–Yan process: A closer look at higher twist effects, *Phys. Rev. Lett.* 73(7), 939 (1994)
78. K. J. Eskola, P. Hoyer, M. Vänttinen, and R. Vogt, Higher-twist effects in the Drell–Yan angular distribution, *Phys. Lett. B* 333(3–4), 526 (1994)
79. J. G. Heinrich, C. Biino, J. F. Greenhalgh, W. C. Louis, K. T. McDonald, S. Palestini, D. P. Russell, F. C. Shoemaker, A. J. S. Smith, C. E. Adolphsen, J. P. Alexander, K. J. Anderson, J. S. Conway, J. E. Pilcher, A. Possoz, and E. I. Rosenberg, Higher-twist effects in the reaction $\pi^- N \to \mu^+\mu^- X$ at 253 GeV/c, *Phys. Rev. D* 44(7), 1909 (1991)
80. E. L. Berger and S. J. Brodsky, Quark structure functions of mesons and the Drell–Yan process, *Phys. Rev. Lett.* 42(15), 940 (1979)
81. E. L. Berger, Quark structure functions of Mesons, fragmentation functions, higher twist effects in QCD, deep inelastic scattering, and the Drell–Yan process, *Z. Phys. C* 4, 289 (1980)
82. E. L. Berger, Higher-twist effects in deep-inelastic scattering, *Phys. Lett. B* 89(2), 241 (1980)
83. D. Boer, Investigating the origins of transverse spin asymmetries at BNL RHIC, *Phys. Rev. D* 60(1), 014012 (1999), arXiv: hep-ph/9902255
84. X. Ji, J. P. Ma, and F. Yuan, QCD factorization for spin-dependent cross sections in DIS and Drell–Yan processes at low transverse momentum, *Phys. Lett. B* 597(3–4), 299 (2004), arXiv: hep-ph/0405085
85. J. Zhou, F. Yuan, and Z. T. Liang, Drell–Yan lepton pair azimuthal asymmetry in hadronic processes, *Phys. Lett. B* 678(3), 264 (2009), arXiv: 0901.3601 [hep-ph]
86. A. Bianconi and M. Radici, Monte Carlo simulation of events with Drell–Yan lepton pairs from antiproton-proton collisions, *Phys. Rev. D* 71(7), 074014 (2005), arXiv: hep-ph/0412368
87. Z. Lu and B. Q. Ma, Azimuthal asymmetry in unpolarized $\pi N$ Drell–Yan process, *Phys. Lett. B* 615(3–4), 200 (2005), arXiv: hep-ph/0504184
88. A. Bianconi and M. Radici, Monte Carlo simulation of events with Drell–Yan lepton pairs from antiproton-proton collisions: The fully polarized case, *Phys. Rev. D* 72(7), 074013 (2005), arXiv: hep-ph/0504261
89. A. Sissakian, O. Shevchenko, A. Nagaytsev, and O. Ivanov, Direct extraction of transversity and its accompanying T-odd distribution from the unpolarized and single-polarized Drell–Yan processes, *Phys. Rev. D* 72(5), 054027 (2005), arXiv: hep-ph/0505214
90. L. P. Gamberg and G. R. Goldstein, "T-odd effects" in unpolarized Drell–Yan scattering, *Phys. Lett. B* 650(5–6), 362 (2007), arXiv: hep-ph/0506127
91. A. Sissakian, O. Shevchenko, A. Nagaytsev, O. Denisov, and O. Ivanov, Transversity and its accompanying T-odd distribution from Drell–Yan processes with pion-proton collisions, *Eur. Phys. J. C* 46(1), 147 (2006), arXiv: hep-ph/0512095
92. V. Barone, Z. Lu, and B. Q. Ma, The $\cos 2\phi$ asymmetry of Drell–Yan and $J/\phi$ production in unpolarized pp scattering, *Eur. Phys. J. C* 49(4), 967 (2007), arXiv: hep-ph/0612350
93. Z. Lu, B. Q. Ma, and I. Schmidt, Transverse spin effects of sea quarks in unpolarized nucleons, *Phys. Rev. D* 75(1), 014026 (2007), arXiv: hep-ph/0701255
94. P. E. Reimer, Exploring the partonic structure of hadrons through the Drell–Yan process, *J. Phys. G* 34(7), S107 (2007), arXiv: 0704.3621 [nucl-ex]
95. G. A. Miller, Densities, parton distributions, and measuring the nonspherical shape of the nucleon, *Phys. Rev. C* 76(6), 065209 (2007), arXiv: 0708.2297 [nucl-th]
96. B. Zhang, Z. Lu, B. Q. Ma, and I. Schmidt, Extracting Boer–Mulders functions from $p + D$ Drell–Yan processes, *Phys. Rev. D* 77(5), 054011 (2008), arXiv: 0803.1692 [hep-ph]

97. A. Bianconi, A scheme for fast exploratory simulation of azimuthal asymmetries in Drell–Yan experiments at intermediate energies, *Nucl. Instrum. Meth. A* 593(3), 562 (2008), arXiv: 0806.0946 [hep-ex]

98. A. Sissakian, O. Shevchenko, A. Nagaytsev, and O. Ivanov, Transversity and T-odd PDFs from Drell–Yan processes with $pp$, $pD$ and $DD$ collisions, arXiv: 0807.2480 [hep-ph]

99. Z. Lu and I. Schmidt, Updating Boer–Mulders functions from unpolarized $pd$ and $pp$ Drell–Yan data, *Phys. Rev. D* 81(3), 034023 (2010), arXiv: 0912.2031 [hep-ph]

100. V. Barone, S. Melis, and A. Prokudin, Azimuthal asymmetries in unpolarized Drell–Yan processes and the Boer–Mulders distributions of antiquarks, *Phys. Rev. D* 82(11), 114025 (2010), arXiv: 1009.3423 [hep-ph]

101. Z. Lu and I. Schmidt, The cos2$\phi$ azimuthal asymmetry of unpolarized dilepton production at the Z pole, *Phys. Rev. D* 84(9), 094002 (2011), arXiv: 1107.4693 [hep-ph]

102. T. B. Liu and B. Q. Ma, The cos2$\phi$ azimuthal asymmetry of unpolarized $p\bar{p}$ collisions at Tevatron, *Eur. Phys. J. C* 73, 2291 (2013), arXiv: 1201.2472 [hep-ph]

103. T. Liu and B. Q. Ma, Azimuthal asymmetries in lepton-pair production at a fixed-target experiment using the LHC beams (AFTER), *Eur. Phys. J. C* 72(6), 2037 (2012), arXiv: 1203.5579 [hep-ph]

104. L. Y. Zhu, et al. (NuSea Collaboration), Measurement of angular distributions of Drell–Yan dimuons in $p+d$ interactions at 800 GeV/c, *Phys. Rev. Lett.* 99(8), 082301 (2007), arXiv: hep-ex/0609005

105. L. Y. Zhu, et al. (NuSea Collaboration), Measurement of angular distributions of Drell–Yan dimuons in $p+p$ interactions at 800 GeV/c, *Phys. Rev. Lett.* 102(18), 182001 (2009), arXiv: 0811.4589 [nucl-ex]

106. S. J. Brodsky and F. Yuan, Single transverse-spin asymmetries at large $x$, *Phys. Rev. D* 74(9), 094018 (2006)

107. M. Anselmino, M. Boglione, U. D'Alesio, A. Kotzinian, F. Murgia, and A. Prokudin, Role of Cahn and Sivers effects in deep inelastic scattering, *Phys. Rev. D* 71(7), 074006 (2005), arXiv: hep-ph/0501196

108. A. Bacchetta, M. Boglione, A. Henneman, and P. J. Mulders, Bounds on transverse momentum dependent distribution and fragmentation functions, *Phys. Rev. Lett.* 85(4), 712 (2000), arXiv: hep-ph/9912490

109. V. Barone, S. Melis, and A. Prokudin, Boer–Mulders effect in unpolarized SIDIS: An analysis of the COMPASS and HERMES data on the cos2$\phi$ asymmetry, *Phys. Rev. D* 81(11), 114026 (2010), arXiv: 0912.5194 [hep-ph]

110. U. D'Alesio and F. Murgia, Parton intrinsic motion in inclusive particle production: Unpolarized cross sections, single spin asymmetries, and the Sivers effect, *Phys. Rev. D* 70(7), 074009 (2004), arXiv: hep-ph/0408092

111. P. Schweitzer, T. Teckentrup, and A. Metz, Intrinsic transverse parton momenta in deeply inelastic reactions, *Phys. Rev. D* 81(9), 094019 (2010), arXiv: 1003.2190 [hep-ph]

112. A. Airapetian, et al. (HERMES Collaboration), Azimuthal distributions of charged hadrons, pions, and kaons produced in deep-inelastic scattering off unpolarized protons and deuterons, *Phys. Rev. D* 87, 012010 (2013), arXiv: 1204.4161 [hep-ex]

113. M. Osipenko, et al. (CLAS Collaboration), Measurement of semi-inclusive $\pi^+$ electroproduction off the proton, *Phys. Rev. D* 80(3), 032004 (2009), arXiv: 0809.1153 [hep-ex]

114. C. Adolph, et al. (COMPASS Collaboration), Measurement of azimuthal hadron asymmetries in semi-inclusive deep inelastic scattering off unpolarised nucleons, *Nucl. Phys. B* 886, 1046 (2014), arXiv: 1401.6284 [hep-ex]

115. R. N. Cahn, Azimuthal dependence in leptoproduction: A simple parton model calculation, *Phys. Lett. B* 78(2–3), 269 (1978)

116. R. N. Cahn, Critique of parton-model calculations of azimuthal dependence in leptoproduction, *Phys. Rev. D* 40(9), 3107 (1989)

117. H. Georgi and H. D. Politzer, Clean tests of quantum chromodynamics in $\mu p$ scattering, *Phys. Rev. Lett.* 40(1), 3 (1978)

118. A. Méndez, QCD predictions for semi-inclusive and inclusive leptoproduction, *Nucl. Phys. B* 145(1), 199 (1978)

119. A. König and P. Kroll, A realistic calculation of the azimuthal asymmetry in semi-inclusive deep inelastic scattering, *Z. Phys. C* 16(1), 89 (1982)

120. J. Chay, S. D. Ellis, and W. J. Stirling, Azimuthal asymmetry in lepton-proton scattering at high energies, *Phys. Rev. D* 45(1), 46 (1992)

121. J. C. Collins, Fragmentation of transversely polarized quarks probed in transverse momentum distributions, *Nucl. Phys. B* 396(1), 161 (1993)

122. M. Anselmino, M. Boglione, A. Prokudin, and C. Turk, Semi-inclusive deep inelastic scattering processes from small to large $P_T$, *Eur. Phys. J. A* 31(3), 373 (2007), arXiv: hep-ph/0606286

123. J. Chay, S. Ellis, and W. Stirling, Azimuthal asymmetry in lepton-proton scattering at high energies, *Phys. Rev. D* 45(1), 46 (1992)

124. K. A. Oganessyan, H. R. Avakian, N. Bianchi, and P. Di Nezza, Investigations of azimuthal asymmetry in semi-inclusive leptoproduction, *Eur. Phys. J. C* 5(4), 681 (1998)

125. L. P. Gamberg, G. R. Goldstein, and K. A. Oganessyan, Novel transversity properties in semi-inclusive deep inelastic scattering, *Phys. Rev. D* 67, 071504(R) (2003)

126. L. P. Gamberg, Transversity of quarks and nucleons in SIDIS and Drell Yan, arXiv: hep-ph/0412367

127. V. Barone, Z. Lu, and B. Q. Ma, On the cos2$\phi$ asymmetry in unpolarized leptoproduction, *Phys. Lett. B* 632(2–3), 277 (2006), arXiv: hep-ph/0512145

128. V. Barone, A. Prokudin, and B. Q. Ma, Systematic phenomenological study of the cos2$\phi$ asymmetry in unpolarized semi-inclusive DIS, *Phys. Rev. D* 78(4), 045022 (2008), arXiv: 0804.3024 [hep-ph]

129. M. Boglione, S. Melis, and A. Prokudin, Partonic transverse motion in unpolarized semi-inclusive deep inelastic scattering processes, *Phys. Rev. D* 84(3), 034033 (2011), arXiv: 1106.6177 [hep-ph]

130. B. Pasquini and P. Schweitzer, Naive time-reversal odd phenomena in semi-inclusive deep-inelastic scattering from light-cone constituent quark models, *Phys. Rev. D* 83(11), 114044 (2011)

131. V. Barone, M. Boglione, J. O. Gonzalez Hernandez, and S. Melis, A phenomenological analysis of azimuthal asymmetries in unpolarized semi-inclusive deep inelastic scattering, *Phys. Rev. D* 91, 074019 (2015), arXiv: 1502.04214 [hep-ph]

132. E. Christova and E. Leader, Tests of the extraction of the Sivers, Boer–Mulders and transversity distributions in SIDIS reactions, arXiv: 1507.01399 [hep-ph]

133. B. Zhang, Z. Lu, B. Q. Ma, and I. Schmidt, cos2$\phi$ asymmetries in unpolarized semi-inclusive DIS, *Phys. Rev. D* 78(3), 034035 (2008), arXiv: 0807.0503 [hep-ph]

134. J. Breitweg, et al. (ZEUS Collaboration), Measurement of azimuthal asymmetries in deep inelastic scattering, *Phys. Lett. B* 481(2–4), 199 (2000)

135. M. Burkardt, Hadron tomography, *Int. J. Mod. Phys. A* 21(04), 926 (2006), arXiv: hep-ph/0509316

136. F. Giordano,et al. (HERMES Collaboration), Measurement of azimuthal asymmetries of the unpolarized cross section at HERMES, *AIP Conf. Proc.* 1149, 423 (2009), arXiv: 0901.2438 [hep-ex]

137. W. Käfer (COMPASS Collaboration), Measurements of unpolarized azimuthal asymmetries at COMPASS, arXiv: 0808.0114 [hep-ex]

138. A. Bressan (COMPASS Collaboration), Azimuthal asymmetries in SIDIS off unpolarized targets at COMPASS, arXiv: 0907.5511 [hep-ex]

139. M. Anselmino, M. Boglione, U. D'Alesio, A. Kotzinian, S. Melis, F. Murgia, A. Prokudin, and C. Turk, Sivers effect for pion and kaon production in semi-inclusive deep inelastic scattering, *Eur. Phys. J. A* 39(1), 89 (2009), arXiv: 0805.2677 [hep-ph]

140. M. Anselmino, M. Boglione, U. D'Alesio, A. Kotzinian, F. Murgia, A. Prokudin, and S. Melis, Update on transversity and Collins functions from SIDIS and data, *Nucl. Phys. B Proc. Suppl.* 191, 98 (2009), arXiv: 0812.4366 [hep-ph]

141. D. Boer, Sudakov suppression in azimuthal spin asymmetries, *Nucl. Phys. B* 603(1–2), 195 (2001), arXiv: hep-ph/0102071

142. S. M. Aybat, J. C. Collins, J. W. Qiu, and T. C. Rogers, QCD evolution of the Sivers function, *Phys. Rev. D* 85(3), 034043 (2012), arXiv: 1110.6428 [hep-ph]

143. S. M. Aybat, A. Prokudin, and T. C. Rogers, Calculation of transverse-momentum-dependent evolution for Sivers transverse single spin asymmetry measurements, *Phys. Rev. Lett.* 108(24), 242003 (2012), arXiv: 1112.4423 [hep-ph]

144. M. G. Echevarria, A. Idilbi, A. Schaefer, and I. Scimemi, Model independent evolution of transverse momentum dependent distribution functions (TMDs) at NNLL, *Eur. Phys. J. C* 73(12), 2636 (2013), arXiv: 1208.1281 [hep-ph]

145. P. Sun and F. Yuan, Transverse momentum dependent evolution: Matching semi-inclusive deep inelastic scattering processes to Drell–Yan and W/Z boson production, *Phys. Rev. D* 88(11), 114012 (2013), arXiv: 1308.5003 [hep-ph]

146. Z. B. Kang, A. Prokudin, P. Sun, and F. Yuan, Nucleon tensor charge from Collins azimuthal asymmetry measurements, *Phys. Rev. D* 91(7), 071501 (2015), arXiv: 1410.4877 [hep-ph]

147. S. J. Brodsky, F. Fleuret, C. Hadjidakis, and J. P. Lansberg, Physics opportunities of a fixed-target experiment using LHC beams, *Phys. Rep.* 522(4), 239 (2013), arXiv: 1202.6585 [hep-ph]

148. V. D. Burkert, The JLab 12 GeV upgrade and the initial science program, *Proc. Int. Sch. Phys. Fermi* 180, 303 (2012), arXiv: 1203.2373 [nucl-ex]

149. D. Boer, M. Diehl, R. Milner, R. Venugopalan, W. Vogelsang, et al., Gluons and the quark sea at high energies: Distributions, polarization, tomography, arXiv: 1108.1713 [nucl-th]

150. A. Accardi, J. L. Albacete, M. Anselmino, N. Armesto, E. C. Aschenauer, et al., Electron Ion Collider: The next QCD frontier - Understanding the glue that binds us all, arXiv: 1212.1701 [nucl-ex]